REPORT NO. RE-TR-62-10

COPY 9

SOME OPTICAL CONTRAST SEEKER SYSTEM CONSIDERATIONS

31 December 1962

U S ARMY MISSILE COMMAND
REDSTONE ARSENAL, ALABAMA

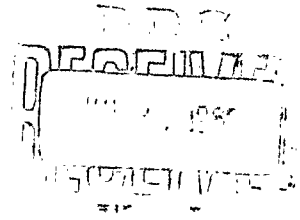

DESTRUCTION NOTICE

Destroy, do not return.

31 December 1962

Report No. RE-TR-62-10

SOME OPTICAL CONTRAST SEEKER SYSTEM CONSIDERATIONS

by

G. Willems

DA Project No. 1-D-22-901-A-204
AMCMS Code No. 5221.11.146

Correlation Branch
Electromagnetics Laboratory
Directorate of Research and Development
U. S. Army Missile Command
Redstone Arsenal, Alabama

ABSTRACT

Some elementary problems peculiar to a ground-to-ground homing missile system are discussed. The work is specifically oriented toward the application of a television guidance sensor of the contrast contour type to an anti-tank weapon. The design of a simple laboratory TV servo-tracker is presented. Appendices A and B discuss test vehicles for subject applications and present pertinent XQ-2 drone parameters.

TABLE OF CONTENTS

LIST OF ILLUSTRATIONS

LIST OF ILLUSTRATIONS (Concluded)

SOME OPTICAL CONTRAST SEEKER

SYSTEM CONSIDERATIONS

I. INTRODUCTION

The employment of passive seekers of the television (raster-scan) type as the error sensing element in a collision-seeking (homing) missile presents many peculiar problems. A thorough investigation of the system application of such a seeker dictates the need for specific information in the following areas:

1. Acquisition and identification of targets.

2. Optimum selection of optics and sensor and evaluation of the limitations imposed by the operating environment.

3. Signal processing techniques for acquisition, track, stability and communication (if needed).

4. Practical seeker design specifications to meet dynamic requirements and impose minimum size and weight requirements on the missile.

5. Missile navigation and flight dynamics which relate to seeker requirements.

This report covers the work done to date on areas 4 and 5. Additional related work has been reported in Report No. RE-TR-63-3.

For purposes of limiting the number of system parameters, a fixed-range ground-to-ground, line-of-sight (LOS) tank engagement was assumed. Within this framework, simplified mathematical missile models were used in a proportional navigation homing environment for the establishment of gross system requirements, limitations and capabilities. The design data thus generated were used to outline the

requirements of a two-axis servo tracker, and a laboratory model of the tracker has been constructed.

II. SOME ELEMENTARY GEOMETRIC CONSIDERATIONS

In the design of a homing system based on an image contour tracker of the raster-scan type, the angle subtended by the target within the field-of-view becomes interesting for several reasons:

1. At maximum range, the field-of-view of the optics must be sufficiently small to yield a target image large enough to exceed the resolution limitations of the TV seeker.

2. As the missile nears the target, the image will subtend a proportionally larger portion of the field-of-view, until eventually the image-to-field area ratio becomes unity, and tracking information is lost. The missile must then coast unguided to the target. Minimizing this coast range requires a large field-of-view conflicting with resolution requirements.

This conflict may be minimized by using programed variable-field optics at a penalty in cost, weight, complexity, and size. To establish allowable terminal engagement guidance system performance, the trade-offs involved in using fixed field optics were investigated. For this purpose, the magnitude of the angle subtended by a given target as a function of range is required and was determined as follows:

From Figure 1:

$$\theta_t = 2\lambda_t$$

$$\lambda_t = \tan^{-1} \frac{h/2}{R_t}$$

Since λ_t is small for all ranges of interest, the usual small-angle approximations apply. For example, if $h/2 = 5$ ft., λ_t will equal 100 milliradians or 6° at R = 50 feet.

Thus:

$$\lambda_t \approx \frac{h/2}{R_t} = \frac{h}{2R_t}$$

and

$$\theta_t = 2\lambda_t \approx \frac{2h}{2R} \approx \frac{h}{R}$$

It can be seen that θ_t is dependent only on target size and range. Since the above function is a reciprocal function, it is not conveniently plotted on linear graph paper. However, one can make the transformation:

$$\log \theta_t = \log h - \log R .$$

Ignoring the logarithm, the above equation is obviously that of a straight-line (slope-intercept form, $Y = b - mx$). Thus, if the function $\theta_t = h/R$ is plotted on log-log paper, straight-line plots are obtained. The advantages of this form for the given function are:

1. Several decades of the variables of interest are easily plotted with good accuracy.

2. Only three values of each function of interest need be calculated to verify the straight line. Plots of θ_t versus R are shown in Figure 2 for three different target sizes. Note that four decades are used for the ordinate. The family of curves to the right should be referred to the right hand ordinate, the one to the left, to the left hand ordinate.

For the range of fields of view considered appropriate (0.5° to 2°), Figure 2 shows that the coast range could be as great as 1,000 feet if fixed optics are used with the proposed TV tracker-- a contrast contour device (CCT tracker) being built for the Army by the Southern Research Institute. Terminal performance of missile models were evaluated under such conditions, and some preliminary results are reported in a later section.

In addition to θ_t, it might be of interest to know the rate of change of the angle subtended by the target, or $\dot{\theta}_t$. This can be easily determined:

Since, $\theta_t = \frac{h}{R}$,

$$\dot{\theta}_t = \frac{d}{dt}\left(\frac{h}{R}\right) = \frac{h\dot{R}}{R^2} = \frac{hv}{R^2} \text{ or } \frac{\theta v}{R} .$$

Unlike θ_t, $\dot{\theta}_t$ is dependent upon missile velocity. Figures 3 and 4 show plots of $\dot{\theta}_t$ for three target sizes and two missile velocities (750 ft/sec and 1,000 ft/sec, respectively). For the reasons previously indicated, these plots are also made on log-log paper.

Missile velocity was assumed constant throughout each flight for all analyses reported.

Another parameter of interest is the angular turning rate required of a missile in order to track a moving target. Since the maximum rate corresponds to a target moving perpendicularly to the missile flight path, approximate values were obtained thus: At any one instant, the target was considered to be a point moving along the circumference of a circle of radius R (Fig. 5). The target velocity was then V_t, the tangential velocity of the point, and

$$\text{angular velocity of missile} \approx \omega = \frac{V_t}{R},$$

$$\text{angular acceleration of missile} \approx \alpha = \frac{d}{dt}\left(\frac{V_t}{R}\right).$$

$$\alpha = \frac{-V_t \dot{R}}{R^2} = \frac{V_t^2}{R^2} = \omega^2.$$

ω versus R is plotted in Figure 6 and α versus R in Figure 7. In these plots, target velocities of 44 ft/sec and 88 ft/sec are considered. For the 30 mph (44 ft/sec) target, moving perpendicularly to the field of view, the required tracking rates are quite modest to within a very short range from the target. Actual angular rates will include effects of missile dynamics, which will also affect seeker angular rate performance requirements.

III. MISSILE STUDIES

A. Introduction

The objective of the present Optical Contrast Seeker (OCS) program is to demonstrate the feasibility of a homing missile system employing such a seeker, rather than to develop a tactical system design. Many simplifying assumptions are therefore possible and indeed desirable. Preliminary analytical and analog simulation studies were made within the framework of the following limitations:

1. Missile dynamics are represented by a second order transfer function.

2. Planar analysis only is performed.

3. Target engagement is line-of-sight from a stationary launcher.

4. Target is stationary.

B. Navigation Techniques

Homing missiles make use of the observed motion of the missile-target LOS, and several well-known navigation laws are available for selection. Among these are pure pursuit, constant bearing, and proportional navigation. The first two generally require extreme missile maneuvers; for vehicles of limited performance the navigation scheme is the most practical to implement and is thus chosen here (Ref. 1). In proportional navigation, the missile detects any rotation of the line of sight and assumes a turning rate proportional to the line of sight rotation, in the direction which will reduce the LOS rate and thus tend to return to a constant-bearing collison course. In the case of a nonaccelerating target, once the missile has corrected initial errors, the line-of-sight ceases to rotate and the constant bearing course is achieved.

Ideally, proportional navigation can be defined thus: $\dot{\gamma}_M = K\dot{\sigma}$, i.e., the missile turning rate is equal to some constant (usually between 2 and 6) times the LOS angular rate. A high value of K relates to loop gain and generally yields an oscillatory trajectory. On the other hand for K = 2, it can be shown mathematically that the required missile acceleration is no longer bounded and approaches infinity as the range approaches zero (Ref. 1).

If a second order missile and first order lag for the seeker are assumed, the guidance equation would become:

$$\dot{\gamma}_M = K\left(\frac{1}{\frac{S^2}{\omega_n^2} + \frac{2\zeta}{\omega_n}S + 1}\right)\left(\frac{1}{1 + \tau_1 S}\right)\dot{\sigma} .$$

This equation can be derived from a differential equation analysis: Assumed approximate missile behavior:

$$\ddot{\alpha} + 2\zeta\omega_n\dot{\alpha} + \omega_n^2\alpha = \omega_n^2 K_1\delta$$

where $K_1\delta$ relates to missile control effectiveness. Replacing d/dt by S and dividing through by ω_n^2:

$$\alpha\left(\frac{S^2}{\omega_n^2} + \frac{2\zeta}{\omega_n}S + 1\right) = K_1\delta \text{ or } \frac{\alpha}{\delta} = \frac{K_1}{\frac{S^2}{\omega_n^2} + \frac{2\zeta}{\omega_n}S + 1} . \qquad (A)$$

Assuming the seeker equation with 1st order lag:

$$\tau_1\dot{\delta} + \delta = K\dot{\sigma}$$

or

$$\delta(1 + \tau_1 S) = K\sigma S, \text{ or } \delta = \frac{K\sigma S}{1 + \tau_1 S} .$$

Inserting δ into Equation A and transposing terms in order to obtain the α/σ transfer function:

$$\frac{\alpha}{\sigma} = \left(\frac{KK_1}{\frac{S^2}{\omega_n^2} + \frac{2\zeta}{\omega_n} S + 1}\right)\left(\frac{S}{1 + \tau_1 S}\right). \qquad \text{(B)}$$

Introducing the approximate lift equation:

$$\dot{\gamma}_M = \frac{\alpha}{\tau_2} \text{ where } \tau_2 \text{ is assumed constant, or } \alpha = \dot{\gamma}_M \tau_2 .$$

Inserting above value of α into Equation B the desired $\dot{\gamma}_M/\sigma$ transfer function is obtained:

$$\frac{\dot{\gamma}_M}{\sigma} = \left(\frac{\frac{KK_1}{\tau_2}}{\frac{S^2}{\omega_n^2} + \frac{2\zeta}{\omega_n} S + 1}\right)\left(\frac{S}{1 + \tau_1 S}\right)$$

The above expression has the same form as the original equation. By transposing σ to the right side and combining it with the free S, σS or $\dot{\sigma}$ is obtained.

The block diagram of this simple homing loop is shown in Figure 8, and the analog simulation program for one plane (yaw) in Figure 9. Several elementary observations can be made from Figure 8:

1. The system is of the 4th order, and thus the loop will inevitably become unstable if the gain becomes high enough. This is due to the fact that the eventual contribution of a 4th order system will be 360° of phase lag. However, provided $1/\tau_1$ is greater than the natural frequency of the missile, the total phase lag in some region below ω_n is less than 180°, and the system will operate stably in this region.

2. Assuming that small angle approximations are valid, σ is given by y/R. This means that as R approaches 0, y/R approaches ∞ and the system will of necessity become unstable. Thus, for a given missile performance, the choice of navigation constant K becomes a matter of trade-offs between launch and terminal performance. The initial gain must be high enough so that dispersion is minimized, yet low enough so that the system does not become unstable prematurely.

3. The navigation constant K tends to lose explicit meaning in this type of simulation. All the constants K, K_1, τ_2, are lumped together

as a factor relating to the loop gain. Only when specific performance numbers are assigned to the missile (K_1, τ_2), does K become meaningful. For convenience in mechanizing the simulation, K was assumed to be 3, and K_1/τ_2 (λ in Figure 9) was varied.

C. Investigation of Fixed Versus Gimballed Seeker

An early simulation study was required in order that an expeditious decision could be made as to whether a constant field of view seeker could be body fixed. The dominant requirement of a body-fixed tracker is that the missile center-line (or other longitudinal reference) form an angle with the LOS not greater than the field of view throughout the flight; otherwise, the target will leave the field of view and tracking will terminate. At the time this information was desired, it was believed that a field of view of ± 2° might be feasible and the studies performed on this basis. A much smaller field of view is now required to allow the CCT tracker to resolve tank-sized targets at maximum range. However, it was determined that even a ± 2° field of view would not allow employment of a body-fixed seeker unless some stringent missile launch dispersion restrictions were met. For the smaller field of view, a servo-directed seeker sensor is a definite requirement.

For the purpose of investigating launch dynamics, a series of simulated trajectories were obtained for the yaw plane. Figure 10, showing pertinent geometry, indicates that the angle $\alpha + \gamma$ is of the greatest interest. $\beta(\beta = \sigma)$ can be neglected since it is generally small and its peak value occurs after α and γ have been reduced considerably. The fixed parameters used in the runs were:

R_O = initial range = 6,000 feet

$\dot{Y}_O$ = initial cross velocity = 50 ft/sec

τ_1 = seeker time constant = 0.03 sec

K = navigation constant = 3

Stationary target

The initial cross-velocity of 50 ft/sec was selected to take care of all dispersions that might be encountered. This value is less than 5 per cent of the missile velocities selected and is considered to be a realistic estimate. All other parameters were varied and are tabultated in Table I. It was found from the simulator runs that the $\dot{Y}_O$ used resulted in an initial γ that did not change noticeably for a few hundred feet. The peak transient value of α occurred generally at $T < 0.3$ seconds; thus the maximum angle between missile centerline and target can be

approximated by $(\alpha + \gamma_o + \beta) \approx (\alpha + \gamma_o)$. Table I shows that without exception, all angles exceed the 2° half-angle of the assumed 4° body-fixed seeker.

No analysis was made of terminal guidance in this study. Guidance was terminated and the controls locked when the missile was 50 feet from target. This distance was arbitrarily selected and for this reason many of the runs resulted in quite unstable terminal trajectories. Thus the miss-distance column of Table I is not too meaningful, and for those runs where the oscillations were very large (i.e., loop became quite unstable) prior to the 50-foot range, no values were entered. The basic reason for omitting terminal guidance in this study is based on the fact that for small fields of view tracking information will be lost in the terminal phase and the missile will coast without guidance as previously discussed.

As a result of these simple investigations, some preliminary conclusions may be hazarded:

1. Unless a fixed seeker with a half-angle of at least 5° to 7° is feasible, further consideration should be given only to gimballed seeker sensors. Subsequent work is based on this conclusion.

2. Launch dynamics place performance requirements that are not unreasonable on the servo tracker. A typical peak value of 2° for an underdamped ($\zeta = 0.2$) missile may be reached in a maximum of 0.1 sec. An approximate $\dot{\alpha}$ of 20°/sec then results, and we must track at least at that rate to stay on target. At this time it seems that a gross minimum $\dot{\alpha}$ value of 30°/sec would be adequate as a specification provided further guidance studies do not dictate otherwise. A more accurate requirement can be determined only for well defined missile performance parameters. Higher rates up to 60°/sec should be achievable without undue difficulty if necessary.

D. Stability Considerations

A detailed stability analysis of any feedback control system requires specific dynamic performance of each element of the control loop, including nonlinearities. The determination of the degree of stability of the homing loop shown in Figure 8 as a function of range can be determined easily but should not be construed as indicating the performance of an actual missile system. Such an analysis at this stage is nevertheless valuable for several reasons:

Table I. LAUNCH DYNAMICS DATA

Missile			γ degree	α degree	$\alpha + \gamma$ degree	Miss distance* ft	Run no.	λ	Remarks
ζ	ω_n	Velocity ft/sec							
0.1	5	1,000	---	---	---	---	1	1	Unstable
0.2	5	1,000	---	---	---	---	2	1	Unstable
0.4	5	1,000	2.6	1.7	4.3	---	3	1	Unstable last 50% of trajectory
0.4	5	1,000	3.1	1.9	5	0.5	4	0.5	
0.2	5	1,000	3.1	2.1	5.2	---	5	0.5	Unstable last 25% of trajectory
0.1	5	1,000	3.1	2.2	5.3	---	6	0.5	Unstable most of trajectory
0.1	10	1,000	3.1	2.2	5.3	3	7	0.5	Slightly oscillatory trajectory
0.2	10	1,000	3.1	2.1	5.2	0.5	8	0.5	
0.4	10	1,000	3.1	1.8	4.9	0	9	0.5	
0.1	10	1,000	2.6	2.1	4.7	---	10	1	Unstable most of flight
0.2	10	1,000	2.6	2	4.6	0.5	11	1	Slightly oscillatory trajectory
0.4	10	1,000	2.6	1.7	4.3	0	12	1	
0.1	20	1,000	2.4	2.1	4.5	0	13	1	Oscillatory at end
0.2	20	1,000	2.4	2	4.4	1	14	1	
0.4	20	1,000	2.4	1.5	3.9	1	15	1	
0.1	20	1,000	2.1	2.1	4.2	1	16	2	Oscillatory flight
0.2	20	1,000	2.1	1.9	4	1	17	2	Terminal oscillation
0.4	20	1,000	2.3	1.5	3.8	1.5	18	2	Terminal oscillation
0.4	20	1,500	1.6	1.5	3.1	2	19	2	Terminal oscillation
0.2	20	1,500	1.6	1.8	3.4	---	20	2	Oscillatory, unstable last 50%
0.2	20	1,500	1.7	1.9	3.6	1	21	1	
0.4	20	1,500	1.7	1.6	3.3	0	22	1	

*See text for comment.

1. Stability analysis of an idealized linear system generally represents what could be called a "best" performance, and a similar physical system could be expected to have poorer response. Thus a broad upper bound of performance can be established.

2. The postulate that tracking information will probably be lost with the OCS tracker loop before loop stability becomes a problem can be verified by correlating the critical loop gain in terms of range with the information shown in Figure 2.

The overall open loop transfer characteristics (HG(S)) of the system shown in Figure 8 are given by:

$$HG(S) = \frac{\frac{KK_1 V \omega_n^2 S}{R\tau_2}}{(S^2 + 2\zeta\,\omega_n\, S + \omega_n^2)(1 + \tau_1 S)\, S^2}$$

The value of loop gain A is given by:

$$A = \frac{KVK_2}{\tau_2 R}$$

If the value of A at which the system goes absolutely unstable is determined, the range at which this occurs is easily computed by means of the above equation since all other terms are known (assumed).

The Routh Stability Criterion (Ref. 2) is probably the easiest means of establishing the value of gain for critical stability. However, if the root locus plots of the various assumed systems are obtained, one can not only obtain the critical gain, but also values of gain (and consequently R) in the stable region. For example, it might be of interest to determine the range at which a damping ratio of 0.1 occurs. For this reason, the root locus method was used in this study. Values of ω_n and ζ were chosen, representing four different missile models; a seeker lag time constant, navigation ratio, and missile performance parameters were assumed for a 1,000-ft/sec missile. The root loci of these systems are shown in Figures 11 through 14, and the values of R for various degrees of stability are shown in Table II. Table III summarizes a comparison of the critical range R_C with the value of R at which a $7\frac{1}{2} \times 7\frac{1}{2}$-foot target image fills various angular fields of view. This elementary analysis tends to support the postulate that the sensor may very well be the limiting element in terminal guidance.

Table II
STABILITY VERSUS RANGE

$\omega_n = 10$		$\omega_n = 20$		
$\zeta = 0.1$	$\zeta = 0.2$	$\zeta = 0.1$	$\zeta = 0.2$	R_i(ft)
1,350	834	52.4	36.4	R_{limit}
2,780	1,610	115	70	$R_{\zeta = 0.1}$
---	2,780	---	112	$R_{\zeta = 0.2}$

Table III
CRITICAL RANGE VERSUS FIELD OF VIEW FOR TYPICAL MISSILES

θ_t degree	Coast range, ft	Critical range			
		$\omega_n = 20$		$\omega_n = 10$	
		$\zeta = 0.1$	$\zeta = 0.2$	$\zeta = 0.1$	$\zeta = 0.2$
0.25	1,720	52.4	36.4	1,350	834
0.5	860	52.4	36.4	1,350	834
1.0	430	52.4	36.4	1,350	834
2.0	215	52.4	36.4	1,350	834

E. Terminal Phase Studies

Since the likelihood that the missile will have to coast into the target for some significant range had been established, the effects on accuracy of this unguided trajectory was interesting. For simplicity, the determination of miss-distance was broken down into two groups: stationary targets and moving targets.

1. Stationary Targets. The definition of proportional navigation implies that detection of the line-of-sight rotation is performed, and this signal is used to correct the missile flight path, the tendency being to approximate the constant bearing course. Therefore, in the case of a stationary target, once initial heading errors are corrected, the line-of-sight ceases to rotate and a constant bearing course is achieved. If $\dot{\sigma}$ is zero, then obviously $\dot{\gamma}$ is also zero, and the missile will remain on the correct collision course throughout the flight (assuming no external disturbances), since no guidance information is needed once a steady state σ value is achieved. Thus the displacement of the initial LOS decreases as a function of time-to-go, becoming zero at T = 0.

The obvious limitation on accuracy during the coasting period on a stationary target is the fact that no error is sensed if the missile deviates from its correct trajectory due to disturbances; these can be broken down into two distinct types: random and drifts. Due to the principle of superposition applicable to linear systems, the effect of each type of disturbance may be evaluated individually and the total effect is obtained if desired by the linear combination of the individual ones.

An evaluation of the effects of random disturbances was performed by superimposing upon the error signal ϵ a random noise signal with a Gaussian distribution about 0. Three amplitude values were selected to correspond to various reasonable signal to noise ratios. Since for a stationary target σ becomes a constant, the summing of a constant rms amplitude noise signal yields a fixed signal to noise ratio.

At the moment guidance is terminated, the missile heading will be given by $\sigma \pm \epsilon$ where σ is the "correct" heading and ϵ is the error caused by the instantaneous noise amplitude at the time of guidance termination. The effect of the heading deviation may be assessed with the help of Figure 15. The maximum amplitude that ϵ may have at the moment guidance is terminated and a target hit is still obtainable:

$$\epsilon = \frac{h/2}{R_C}$$

where

$\frac{h}{2}$ = half of target height

R_C = coast range

Since the peak amplitude and Gaussian distribution of the injected noise are known, the cumulative probability distribution of the noise signal may be plotted as shown in Figures 16 through 18. These plots are for the three selected values of S/N ratios. The percentage of time that ϵ is less than the maximum permissible value can then be read off these curves and an approximation to the hit probability can be obtained.

The primary limitation of this estimate is that a steady state condition for the controlled system is assumed. Although, this is true with respect to the basic error signal (σ = constant at this stage), the system will be in a transient state due to the noise, and the actual output (heading) error could exceed the input considerably due to the damping ratio decrease as a function of lessening range. However, once again

an upper bound for performance is obtained. The predicted hit probabilities for three different coast ranges and signal-to-noise ratios are tabulated in Table IV, along with experimental results obtained as follows: In order to obtain an idea of the accuracy of this prediction, an analog simulation experiment was performed. Approximately 1,000 trajectories were made for each of the conditions in Table V and the total runs and hits counted. The ratio of the two yields the hit probability. A hit was defined as any trajectory within ± 3.5 feet of target at R = 0. A sample recording of part of one of the runs is shown in Figure 19. With the exception of one obvious discrepancy, Table IV shows that fair agreement exists between predicted and experimental values.

Table IV

COMPARISON OF EXPERIMENTAL P_h VERSUS ANALYTICAL PREDICTION

σ = 28 mr	Predicted P_h			Measured P_h		
R_{coast}, ft	S/N = 7	S/N = 3.5	S/N = 2	S/N = 7	S/N = 3.5	S/N = 2
800	0.95	0.6	0.3	0.88	0.7	0.6
400	1.0	0.9	0.7	0.87	0.76	0.65
200	1.0	1.0	0.95	0.9	0.87	0.8

Table V

MAXIMUM ALLOWED ϵ VERSUS COAST RANGE

R_{coast}, ft	Maximum allowable ϵ
800	4.68 mr
400	9.37
200	18.74

Unilateral drifts appear to present the most serious problem during coasting flight. A specification of maximum allowable cumulative drift error is easily obtained. The external drift must impart upon the missile a lateral acceleration no greater than that which will result in a lateral displacement of 3.75 feet at R = 0. This value is given by the following equation:

$$a_d = \frac{2yV^2}{R_c^2} = \frac{7.5V^2}{R_c^2} \qquad \text{for a standard } 7.5 \times 7.5\text{-foot target.}$$

The limit values of a_d for a 1,000 ft/sec-missile velocity and three coast ranges are shown in Table VI.

Table VI
MAXIMUM ALLOWABLE a_d VERSUS COAST RANGE

R_{coast}, ft	a_d, ft/sec^2
800	11.7
400	46.8
200	182.0

2. Moving Targets. The problem of hitting moving or accelerating targets presents the most serious limitation on a weapon that loses guidance information in the closing phases of engagement.

In addition to noise and drift errors, the error caused by the change in target position during the coast period must be added. The magnitude of this error is a function of many parameters, and since the generalized proportional navigation trajectory equations cannot be solved in closed form, a general expression for miss becomes difficult to obtain. Some simulation trajectories for the typical missile transfer functions previously used have indicated that miss distances of 10 feet are obtained against accelerating (4.5 ft/sec^2) targets for an 800-foot coast range. Lesser target accelerations and shorter coast ranges will diminish this error proportionally.

Constant velocity targets present the least problem, since the dynamics involved are very similar to an initial pointing error. Most of the correction is performed early in flight (for a reasonable loop gain) and the miss-distance due to lack of terminal guidance is minimized.

In summarizing, it may be stated that the overwhelming control problem affecting the success of employing a TV contour tracker is guidance loss. Against stationary targets this problem could conceivably be circumvented by a refined missile and guidance system design which would minimize dirft and noise disturbances. Successful engagement of accelerating targets however would seem to require that the coast range be minimized, ideally to negligible distances. An exact quantitative determination of this probability against accelerating targets as a function of miss-distance would require a much more

elaborate analog mechanization than the present simulation and will form part of future work.

It should be pointed out, lest previous statements leave an erroneous impression, that loop instability need not be a limitation on terminal guidance. Modifications of the proportional navigation scheme are possible by the judicious tailoring of loop gain to allow accurate guidance essentially to the impact point. This has been done in the past, particularly in the air-to-air missile field where the dynamic problem is much more severe. The usual approach has been to design the missile and control loop around carefully defined engagement requirements. This of course is necessary within the limits of physical realizability. Additionally, for a missile with limited lateral acceleration, instability may result in limit-cycle oscillation rather than in a diverging trajectory; if the natural frequency is sufficiently high the amplitude of these oscillations can be made quite small. Thus instability need not necessarily result in misses.

IV. SERVO TRACKER DESIGN

Since the high probability has been established that a seeker system utilizing the CCT type of tracker will require a servo gimbal mount, an experimental device was assembled. An existing gimbal system was adapted for use as a laboratory model of a TV tracker. The CCT equipment was not available for this purpose; however, a Walleye type tracker was substituted. This is a point contrast tracker which derives positional information (with respect to an arbitrary reference) by means of slewing vertical and horizontal gates, the intersection of which encloses the target. This device appears adequate for laboratory experiments, provided the expanding target effect due to decreasing range is not required. This sensor has been used to design and evaluate the performance of the basic servo system, since basic error signals similar to the CCT tracker output are available. The existing gimbal system is driven by highly geared DC motors and thus the typical low frequency problem of backlash, stiction, etc. limits performance. A careful quantitative evaluation of the tracking accuracy and its effect in a typical homing engagement has not yet been performed; however, some measurements have been made of tracking performance for a circularly moving target in a plane perpendicular to the sight line. The tracker is shown in Figure 20, and the electronics package in Figure 21. An overall view of the open loop tracking experiment is shown in Figure 22.

In the design of any servo gimbal system, minimum inertia load is desired. Thus, only the vidicon and its deflection coils were mounted initially. However, considerable difficulty was encountered in transmitting the signal to the remotely located preamplifier. This problem was solved by mounting a preamplifier stage with the gimballed vidicon assembly. This has yielded such highly satisfactory results that future assemblies will probably retain this feature.

In designing the servo loop, maximum flexibility was gained by using commercial DC amplifiers of high quality for signal processing and for active compensation networks. This approach was selected because the dynamic characteristics of the CCT tracker are not yet known. Loop gains and compensation network characteristics are easily adjusted in the experimental equipment. Furthermore, if nonlinear gain functions and complex compensation become desirable, these are easily mechanized with the operational amplifiers.

A block diagram of one channel of the servo tracker is shown in Figure 23. The sensor transfer function (Walleye) was determined to have linear DC characteristics, and the dynamic response could be approximated by the first order lag shown in the sensor block. Cancellation compensation was employed, and the lead network pole was placed as far away as possible without excessive attenuation. The motor and gear train transfer function were derived using the usual approximations of linear torque-current characteristics and no gear backlash or stiction. The numerical transfer function was obtained from the formula:

$$\frac{\theta}{V} = S\left[\frac{\frac{K_t}{R_a}}{\frac{K_t K_n}{R_a}\left(\frac{J_m R_a}{K_t K_n} S + 1\right)}\right]$$

where:

K_t = Torque constant

K_n = Back emf constant

R_a = Winding resistance

J_m = Load inertia

N = Gear ratio

The functional schematic diagram of the servo loop is shown in Figure 24, and the power amplifier schematic in Figure 25. The current output versus voltage input for the latter is shown in Figure 26.

Except for the previously mentioned difficulty with slow rates, performance of the laboratory system seems to be adequate. Improvement of the tracking performance in the marginal region by pulse width modulation of the motor driving signal has been investigated but implementation is yet incomplete.

V. CONCLUSIONS

The results of the preliminary analytical and experimental work seem to indicate that the principal problem areas are directly related to the characteristics of the TV raster-scan seeker. Due to the peculiarities of this device, the simple concept of a body-fixed, fixed field optics tracker does not seem feasible. At the minimum, a readily designed gimballed servo mount will be required.

A decisive conclusion cannot yet be reached on the terminal guidance problem. It seems at this time that the field-of-view problem cannot be resolved within the basic seeker itself, since this would require an increase in the resolution of the system.

Future planned work includes careful investigation of the terminal guidance problem employing the dynamics of a typical missile design, such as the MAULER. The results of the investigation should yield quantitative data on miss distance as a function of coast range. If the minimum coast range required by the seeker does not result in acceptable terminal performance, and state-of-art refinements of missile design (if any are possible) do not yield sufficient improvement then the only alternative would seem to be programmed field-of-view optics.

Studies of a higher performance, compact two-axis servo tracker have begun. Under consideration are the following two types:

1. A device employing direct drive electric torque motors, driven by compact, high DC amplifiers.

2. A device employing high performance cold gas pneumatic actuators.

Appendix A

TEST VEHICLE CONSIDERATIONS

A survey has been made of the many missiles and drones, either in existence or in development, to determine the feasibility of using one or more of these as test vehicles. The Ryan Q-2 Firebee drone seems to be a suitable vehicle for open and perhaps closed loop early flight testing. With this possibility in mind, the required aerodynamics and control information has been obtained from Ryan. The equations of motion for this type vehicle have been derived and are shown, along with pertinent numerical data and graphs, in Appendix B.

Since the eventual weight and volume of a flight configuration of the complete CCT seeker cannot be accurately estimated at this time, the selection of a test vehicle for testing in a field environment becomes rather difficult. Therefore, an effort has been initiated to obtain all pertinent information on several missiles in a range of sizes. As these data are obtained, system equations and simulator programs will be written for each missile as was done for the Q-2, and contact maintained with the various contractors so that pertinent changes can be incorporated in the programs. At the present time, effort is being concentrated on the MAULER, which seems to offer rather good possibilities.

Appendix B

LINEARIZED EQUATIONS OF MOTION APPLICABLE TO XQ2-C DRONE

Basic Equations:

1. Force = mass × acceleration
2. Angular acceleration = applied moment/moment of inertia
3. Lift (L) on an airfoil: $L = \frac{1}{2} \rho V^2 S C_L$
   Drag (D) on an airfoil: $D = \frac{1}{2} \rho V^2 S C_D$

Where:

C_L, C_D = dimensionless coefficients

ρ = air density

V = air speed

S = airfoil planform area

Assumptions:

1. Airplane structure is rigid.
2. X, Y, Z coordinates rotate with airplane.
3. Disturbances are small deviations from steady state flight.
4. Longitudinal and lateral equations are decoupled.
   (See Table B-I for symbols and definitions)

Using Newton's Laws:

$$\left.\begin{aligned} m(\dot{U}) &= X - mg \sin\theta \\ m(\dot{V} + Vr &= Y + mg \cos\theta \sin\phi \\ m(\dot{\omega} - Vq &= Z + mg \cos\theta \cos\phi \end{aligned}\right\} \quad \text{I}$$

$$\left.\begin{aligned} L &= I_x\dot{P} - I_{xz}\dot{r} \\ M &= I_y\dot{P} \\ N &= I_z\dot{r} - I_{xz}\dot{P} \end{aligned}\right\} \quad \text{II}$$

Equation I describes translational motions, whereas Equation II denotes angular motions.

Table B-I

DEFINITIONS AND SYMBOLS

Symbol	Definition
X, Y, Z	Forces along X, Y, Z axis
L, M, N	Moments about X, Y, Z axis
U, V, W	Flight path velocities along X, Y, Z axis
p, q, s	Components of angular velocity about X, Y, Z axis
θ	Pitch attitude angle
ϕ	Roll angle
ψ	Yaw angle
γ	Flight path angle
α	Angle of attack
δ_a	Aileron deflection
δ_e	Elevator deflection
δ_r	Rudder deflection
τ	Aircraft time constant
T_v	Change in thrust/unit speed change
V	True air speed
b	Wing span
C	Mean aerodynamic chord
I_{xx}, I_{yy}, I_{zz}	Momenta of inertia about X, Y, Z axis
K_x, K_y, K_z	Radius of gyration about X, Y, Z axis
C_{ij}	Aerodynamic coefficients where first subscript (i) denotes type of forcing function and the second (j) denotes the angle or angular rate associated with the coefficient

Table B-I. (Concluded)

Symbol	Definition
i = m	Pitching moment coefficients
i = n	Rolling moment coefficients
i = L	Lift coefficients
i = l	Yawing moment coefficients
i = y	Side force coefficients

If one assumes small disturbances from steady state flight, the longitudinal equations of motion of an airplane can be written in terms of the stability derivatives:

Lift Equation ($\Sigma F = ma$)

$$m\ddot{Z} = \tfrac{1}{2}\rho V^2 S C_{L\alpha}\alpha + 2(\tfrac{1}{2}\rho V^2 S C_L U).$$

Using the approximation

$$m\ddot{Z} = mV\dot{\gamma}\ ;\ mV\dot{\gamma} = \tfrac{1}{2}\rho V^2 S C_{L\alpha}\alpha + 2(\tfrac{1}{2}\rho V^2 S C_L U)\ .$$

Above equation is more easily applied if rewritten explicitly as a function of the aerodynamic coefficients.

Using the identity $\dot{\theta} = \dot{\gamma} + \dot{\alpha}$ or $\dot{\gamma} = \dot{\theta} - \dot{\alpha}$

$$mV(\dot{\theta} - \dot{\alpha}) = \tfrac{1}{2}\rho V^2 S C_{L\alpha}\alpha + 2(\tfrac{1}{2}\rho V^2 S C_L U)\ .$$

Transposing the left side of equation to the right:

$$(\tfrac{1}{2}\rho V^2 S C_{L\alpha}\alpha) + 2(\tfrac{1}{2}\rho V^2 S C_L U) + mV\dot{\alpha} - mV\dot{\theta} = 0\ .$$

Multiplying through by 2 and dividing by $\rho S V$

$$VC_{L\alpha}\alpha + 2V C_L U + \frac{2m}{\rho S}\dot{\alpha} - \frac{2m}{\rho S}\dot{\theta} = \theta\ .$$

Dividing through by -V:

$$-C_{L\alpha}\alpha - 2C_L U - \frac{2m}{\rho VS}\dot{\alpha} + \frac{2m}{\rho VS}\dot{\theta} = 0\ .$$

The term $\frac{m}{\rho VS}$ has the unit of seconds and can be defined as the air aircraft time constant (τ).

Thus the lift equation becomes:

$$-C_{L\alpha}\alpha - 2C_L U - 2\tau\dot{\alpha} + 2\tau\dot{\theta} = 0. \qquad (A)$$

Moment Equation ($\Sigma M = I\ddot{\theta}$)

$$\tfrac{1}{2}\rho V^2 S C (C_{m\dot{\alpha}}\dot{\alpha} + C_{m\alpha}\alpha - C_{m\dot{\theta}}\dot{\theta} + C_{m\delta e}\delta e) = mk_x^2\ddot{\theta}$$

Multiplying through by 2 and dividing by $\rho V^2 S C$ the following is obtained:

$$C_{m\dot{\alpha}}\dot{\alpha} + C_{m\alpha}\alpha - C_{m\dot{\theta}}\dot{\theta} + C_{m\delta e}\delta e - \frac{2m}{\rho VS}\left(\frac{k_x^2}{VC}\right)\ddot{\theta} = 0 ,$$

where $\frac{m}{\rho VS}$ is again the time constant.

Thus the moment equation can be written:

$$C_{m\dot{\alpha}}\dot{\alpha} + C_{m\alpha}\alpha - C_{m\dot{\theta}}\dot{\theta} + C_{m\delta e}\delta e - 4\tau\left(\frac{C}{2V}\right)\left(\frac{k_x}{C}\right)^2\ddot{\theta} = 0. \qquad (B)$$

The longitudinal flight path equation can be written:

$$V\left[m\dot{U} + T_v U\right] = 2(\tfrac{1}{2}\rho V^2 S)(C_D U + C_L V)$$
$$- \tfrac{1}{2}\rho V^2 S (C_{L\alpha} - C_{D\alpha} - C_{D\theta}) .$$

Multiplying by $\frac{2}{\rho V^2 S}$ and substituting for $\frac{m}{\rho VS}$:

$$- 2\tau\dot{U} + \frac{2\tau}{m} T_v U - 2C_D V - 2C_L U + C_{L\alpha}\alpha - C_{D\alpha}\alpha$$
$$- C_{L\theta}\theta = 0. \qquad (C)$$

The lateral equations can be obtained in the same manner and are given in our standard form:

$$- 2\tau\dot{\beta} + C_{y\beta}\beta + C_L\phi - 2\tau\dot{\psi} = 0 \qquad (D)$$

$$C_{l\beta}\beta - 4\tau\left(\frac{b}{2v}\right)\left(\frac{k_x}{b}\right)^2\ddot{\phi} + C_{L\dot{\phi}}\dot{\phi} + C_{L\dot{\psi}}\dot{\psi} + C_{l\delta a}\delta a = 0 \qquad (E)$$

$$C_{n\beta}\beta + C_{n\dot{\phi}}\dot{\phi} - 4\tau\left(\frac{b}{2v}\right)\left(\frac{k_z}{b}\right)^2\ddot{\psi} + C_{n\dot{\psi}}\dot{\psi} + C_{n\delta r}\delta r = 0 \qquad (F)$$

Equations A through F can then be programmed on the analog computer and are, when properly scaled, valid for the simulation of the Q2C aircraft within the limitations imposed by initial assumptions. However, before the above equations can be conveniently programmed, other assumptions need be made, particularly with respect to the stability derivatives: Many of the derivatives are functions of several variables, such as Mach number, center-of-gravity station, angle of attack, etc. However, most of the derivatives become independent, or at least

linear functions of speed if one restricts himself to speeds below Mach 0.9. One can further simplify the problem by assuming airspeed to be a constant, since most derivatives are then reduced to constants. If more than one speed is of interest, several independent studies can be made for incremental values of airspeed. Assumption must also be made for altitude and payload, since these influence the aircraft time constant (due to ρ) and center of gravity station.

Pertinent data for the Q2-C are shown for three velocities (Mach 0.6, 0.8, and 0.9) in Table B-II. English units are used throughout.

Table B-II

Q-2 NUMERICAL PARAMETERS

Altitude	V = Mach 0.6 Sea level	V = Mach 0.8 Sea level	V = Mach 0.9 5,000 ft
Gross weight	2,060 lb	2,060 lb	2,060 lb
Mass, slugs	64	64	64
ρ	0.00237	0.00237	0.0020
b	12.9 ft	12.9 ft	12.9 ft
S	39.9 ft^2	39.9 ft^2	39.9 ft^2
V	690 ft/sec	920 ft/sec	1,050 ft/sec
τ	1 sec	1 sec	0.85 sec
C_g station	88.5 in	88.5 in	88.5 in
α_o	0.5 deg	0.75 deg	0.7 deg
c	2.783 ft	2.783 ft	2.783 ft
$C_{L\alpha}$ trim	0.067	0.074	0.073
$C_{D\alpha}$	See C_D versus α curves		
T_V	Negligible for jet aircraft		
C_{D_o}	0.002	0.002	0
$C_{L\alpha}$	0.08/deg	0.088/deg	0.085/deg
$C_{m\alpha}$	-0.034/deg	-0.032/deg	-0.032/deg
$C_{m\dot{\alpha}}$	-4.6/rad	-7/rad	-4.2/rad
$C_{m\dot{\theta}}$	-17/rad	-20.1/rad	-16.2/rad

Table B-II (Concluded)

Altitude	V = Mach 0.6 Sea level	V = Mach 0.8 Sea level	V = Mach 0.9 5,000 ft
$C_{m\delta e}$	-02/deg	-0.0181/deg	-0.0165/deg
$C_{y\beta}$	-0.0225/deg	-0.0245/deg	-0.0265/deg
$C_{l\dot{\phi}}$	-0.37/rad	-0.037/rad	-0.037/rad
$C_{l\delta a}$	0.0005/deg	0.00057/deg	0.00055/deg
$C_{n\beta}$	0.0035/deg	0.0038/deg	0.0039/deg
$C_{n\dot{\psi}}$	-0.63/rad	-0.63/rad	-0.73/rad
$C_{n\delta r}$	-0.00077/deg	-0.00075/deg	-0.00075/deg
K_x	0.987 ft	0.987 ft	
K_y	3.89 ft	3.89 ft	
K_z	3.87 ft	3.87 ft	
I_x	62 slug/ft^2	62 slug/ft^2	
I_y	1.036 slug/ft^2	1.036 slug/ft^2	
I_z	1.025 slug/ft^2	1.025 slug/ft^2	
I_{xz}	46.5 slug/ft^2	46.5 slug/ft^2	

The differential equation form is most suitable for analog programming; however, for checking and analysis, the transfer function form is desirable. Derivation of $\theta/\delta_e(S)$, $\phi/\delta_a(S)$ $\psi/\delta_r(S)$ follows: Rewriting the longitudinal equations in operation form, using S = d/dt:

$$(-C_{L\alpha}-2\tau\, S)\,\alpha - 2C_L U + 2\tau\, S\,\theta = 0 \qquad (A')$$

$$(C_{m\dot{\alpha}}\, S + C_{m\alpha})\,\alpha + (-C_{m\dot{\theta}}\, S - \lambda S^2)\,\theta = -C_{m\delta e}\,\delta e \qquad (B')$$

where

$$\lambda = 4\tau\left(\frac{c}{2v}\right)\left(\frac{K_x}{c}\right)^2$$

$$\left[(\eta - 2\tau\, S) - 2C_D - 2C_L\right] U + (C_{L\alpha} - C_{D\alpha})\,\alpha - C_{L\theta} = 0 \qquad (C')$$

where

$$\eta = \frac{2\tau}{m}\, T_v$$

The determinant solution for θ/δ_e is given by:

$$\frac{\theta}{\delta_e}(S) = \frac{\begin{vmatrix} (-C_{L\alpha} - 2\tau S) & -2C_L & 0 \\ (C_{m\dot{\alpha}} S + C_{m\alpha}) & 0 & -C_{m\delta e} \\ (C_{L\alpha} - C_{D\alpha}) & (\eta - 2\tau S - 2C_D - 2C_L) & 0 \end{vmatrix}}{\begin{vmatrix} (-C_{L\alpha} - 2\tau S) & -2C_L & 2\tau S \\ (C_{m\dot{\alpha}} S + C_{m\alpha}) & 0 & (-C_{m\theta} S - \lambda S^2) \\ (C_{L\alpha} - C_{D\alpha}) & (\eta - 2\tau S - 2C_D - 2C_L) & -C_L \end{vmatrix}}$$

The lateral equations can similarly be written:

$$(-2\tau S + C_{y\beta})\,\beta + C_l\,\phi - 2\tau S\,\psi = 0$$

$$C_{l\beta}\,\beta - (\lambda' S^2 - C_{l\dot{\phi}} S)\,\phi + C_{l\dot{\psi}} S\,\psi = -C_{l\delta a}\,\delta a$$

where

$$\lambda' = 4\tau\left(\frac{b}{2v}\right)\left(\frac{K_x}{b}\right)^2$$

$$C_{n\beta}\,\beta + C_{n\dot{\phi}} S\,\phi - (\lambda'' S^2 - C_{n\dot{\psi}} S)\,\psi = -C_{n\delta r}\,\delta r$$

where

$$\lambda'' = 4\tau\left(\frac{b}{2v}\right)\left(\frac{K_z}{b}\right)^2.$$

The determinant solution for $\phi(S)$ is then given by:

$$\phi(S) = \frac{\begin{vmatrix} (-2\tau S + C_{y\beta}) & 0 & -2\tau S \\ C_{L\beta} & -C_{l\delta a}\,\delta a & C_{l\dot{\psi}} S \\ C_{n\beta} & -C_{n\delta r}\,\delta r & -(\lambda'' S^2 - C_{n\dot{\psi}} S) \end{vmatrix}}{\begin{vmatrix} (-2\tau S + C_{y\beta}) & C_l & -2\tau S \\ C_{L\beta} & -(\lambda' S^2 - C_{l\dot{\phi}} S) & C_{l\dot{\psi}} S \\ C_{n\beta} & C_{n\dot{\phi}} S & -(\lambda'' S^2 - C_{n\dot{\psi}} S) \end{vmatrix}}$$

Similarly, $\psi(S)$ becomes:

$$\psi(S) = \frac{\begin{vmatrix} (-2\tau S + C_{y\beta}) & C_l & 0 \\ C_{l\beta} & -(\lambda' S^2 - C_{l\dot{\phi}} S) & -C_{l\delta a}\,\delta a \\ C_{n\beta} & C_{n\dot{\phi}} S & -C_{n\delta r}\,\delta r \end{vmatrix}}{\begin{vmatrix} -(2\tau S + C_{y\beta}) & -C_l & -2\tau S \\ C_{l\beta} & -(\lambda' S^2 - C_{l\dot{\phi}} S) & C_{l\dot{\psi}} S \\ C_{n\beta} & C_{n\dot{\phi}} S & -(\lambda'' S^2 - C_{n\dot{\psi}} S) \end{vmatrix}}$$

The equations derived herein are sufficient for aerodynamics simulation of unsymmetric (bank to turn) vehicles. In the case of the Q2-C drone, all of the required numerical values are available. For a study of the complete loop, including the seeker, the Q2-C autopilot transfer function is required. These additional data are given as follows:

Elevator inner loop:

$$\frac{\delta_e}{\delta_{e_i}} = \frac{1}{\left(1 + \frac{S}{10}\right)\left(1 + \frac{S}{10} + \frac{S^2}{(50)^2}\right)} .$$

Aileron inner loop:

$$\frac{\delta_e}{\delta_{e_i}} = \frac{1}{\left(1 + \frac{S}{5}\right)\left(1 + \frac{S}{100} + \frac{S^2}{(100)^2}\right)} .$$

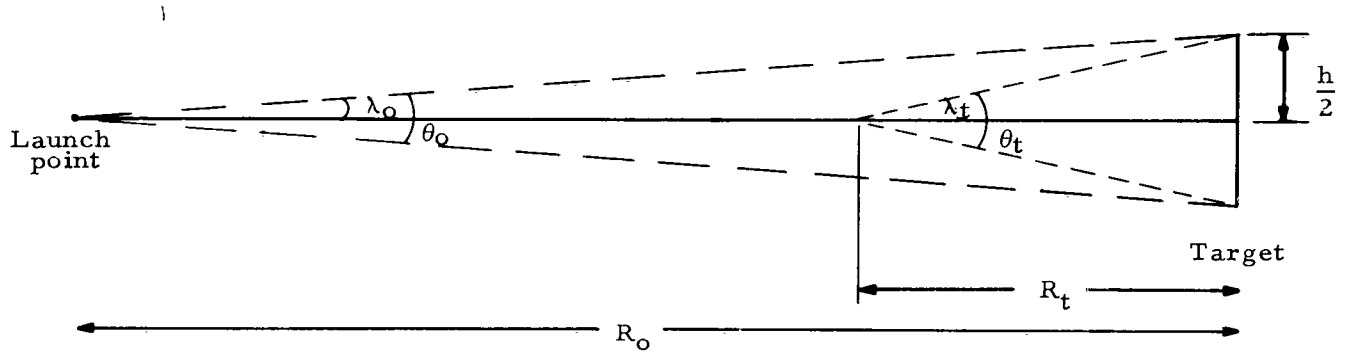

Figure 1. GEOMETRY SHOWING ANGLE SUBTENDED BY TARGET IN FIELD OF VIEW.

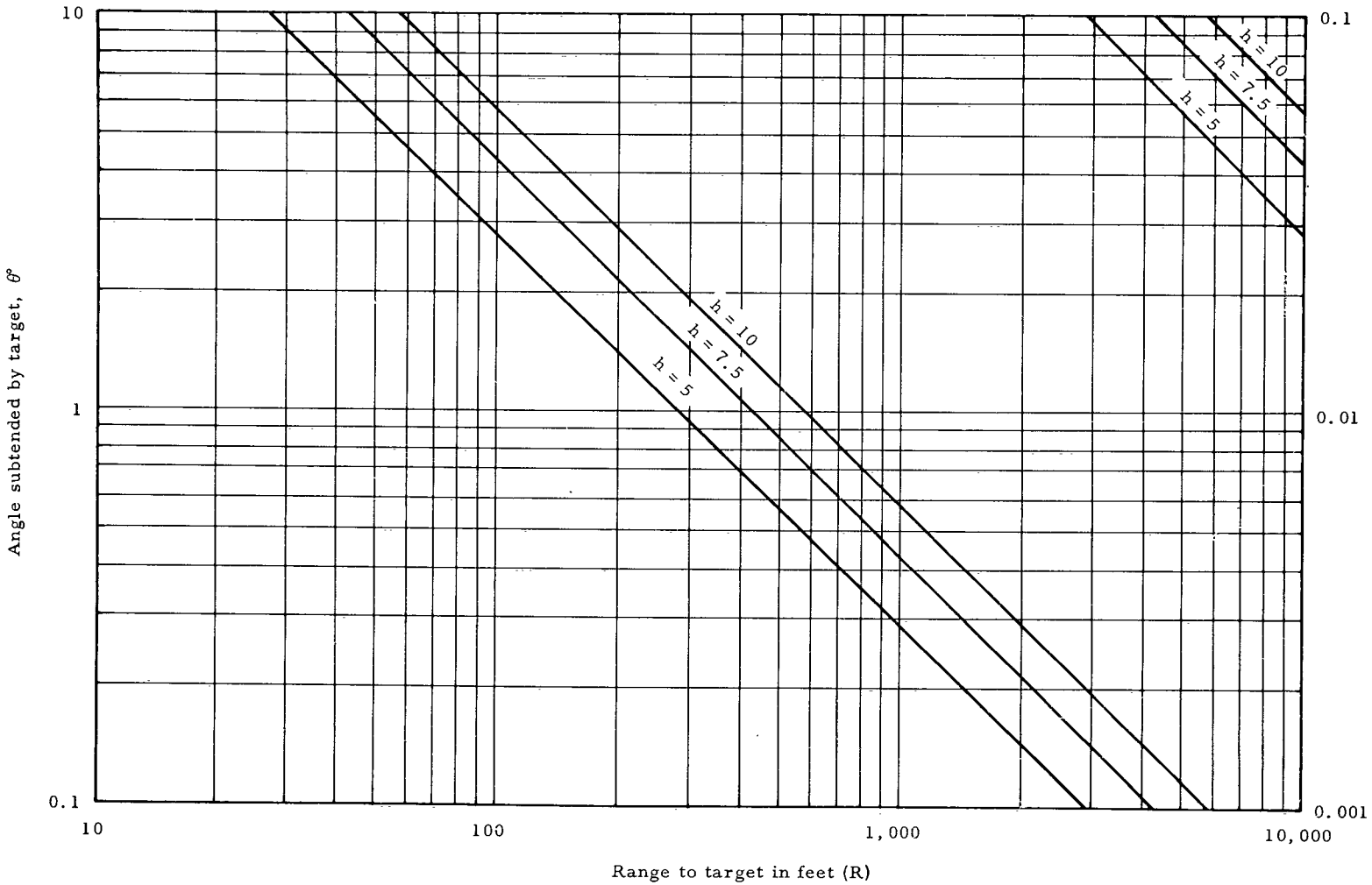

Figure 2. PLOT OF θ_t VERSUS RANGE.

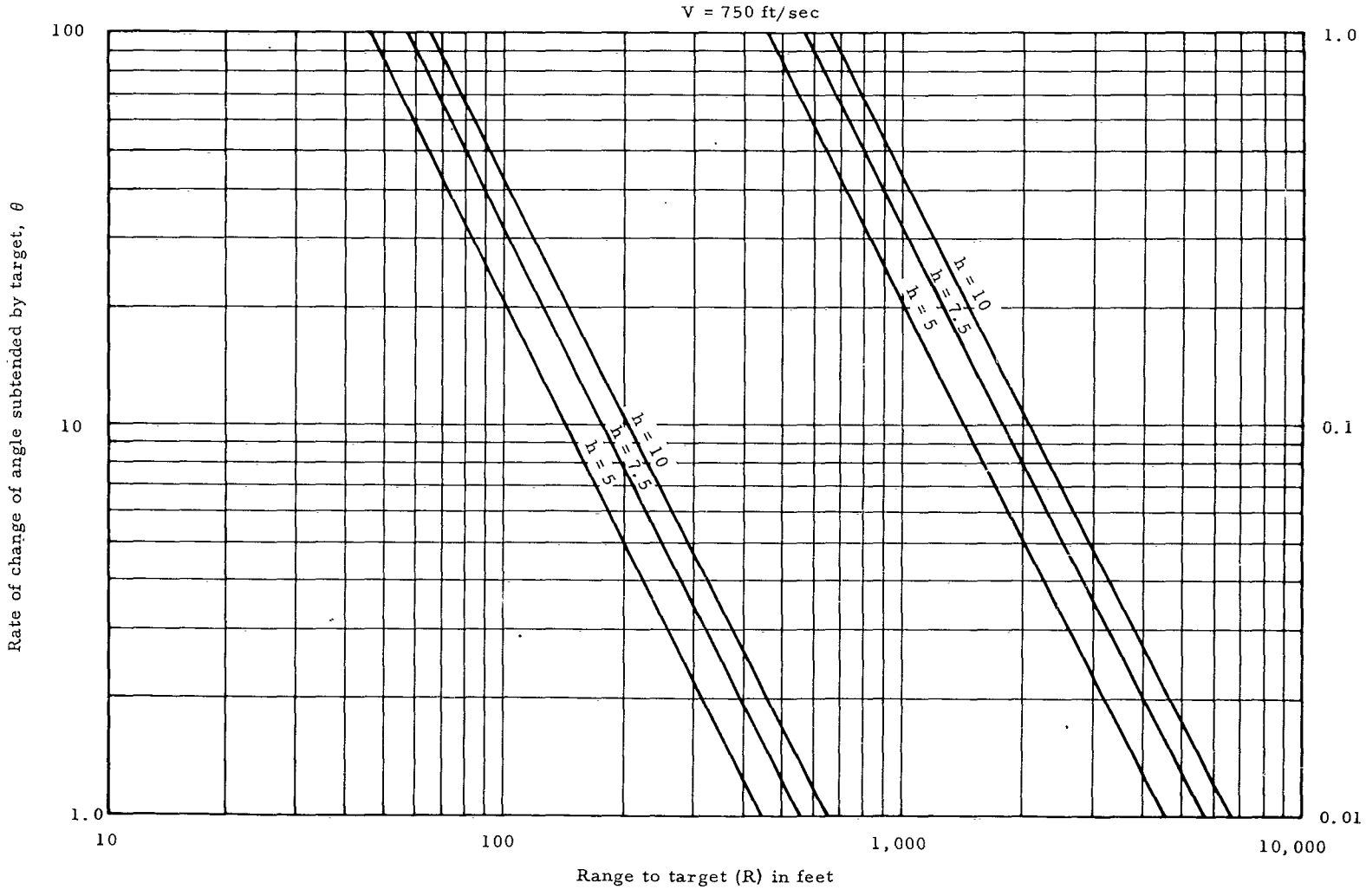

Figure 3. PLOT OF θ_t VERSUS RANGE FOR 750 FEET/SECOND MISSILE.

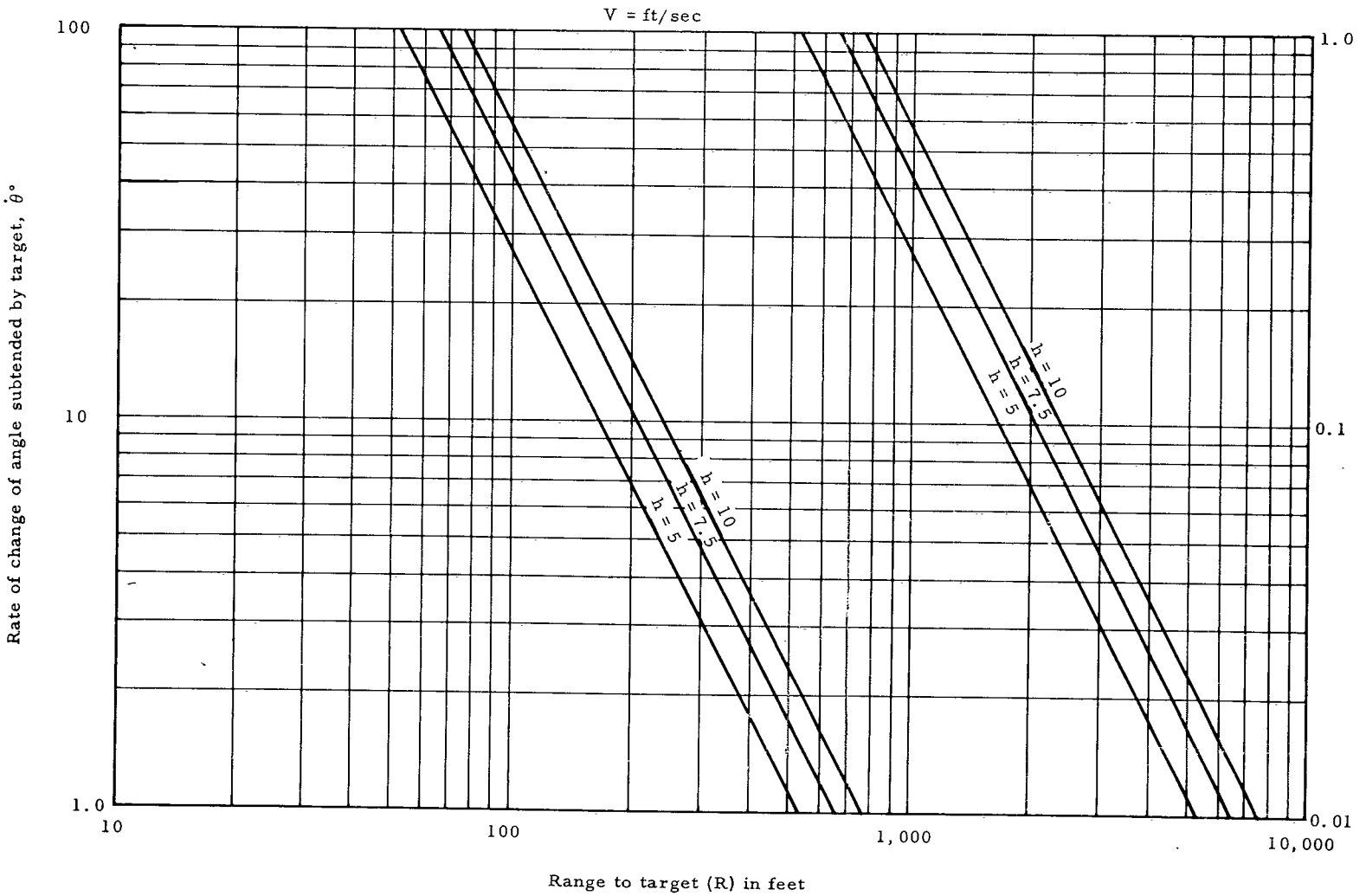

Figure 4. PLOT OF θ_t VERSUS RANGE FOR 1,000 FEET/SECOND MISSILE.

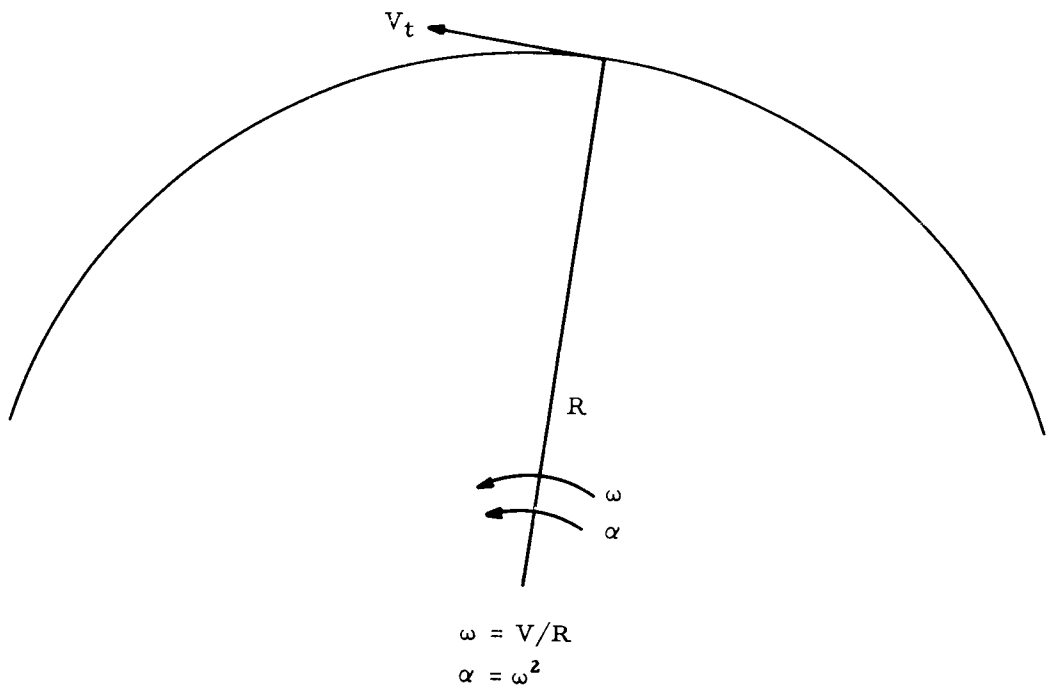

Figure 5. ANGULAR TRACKING RATE GEOMETRY.

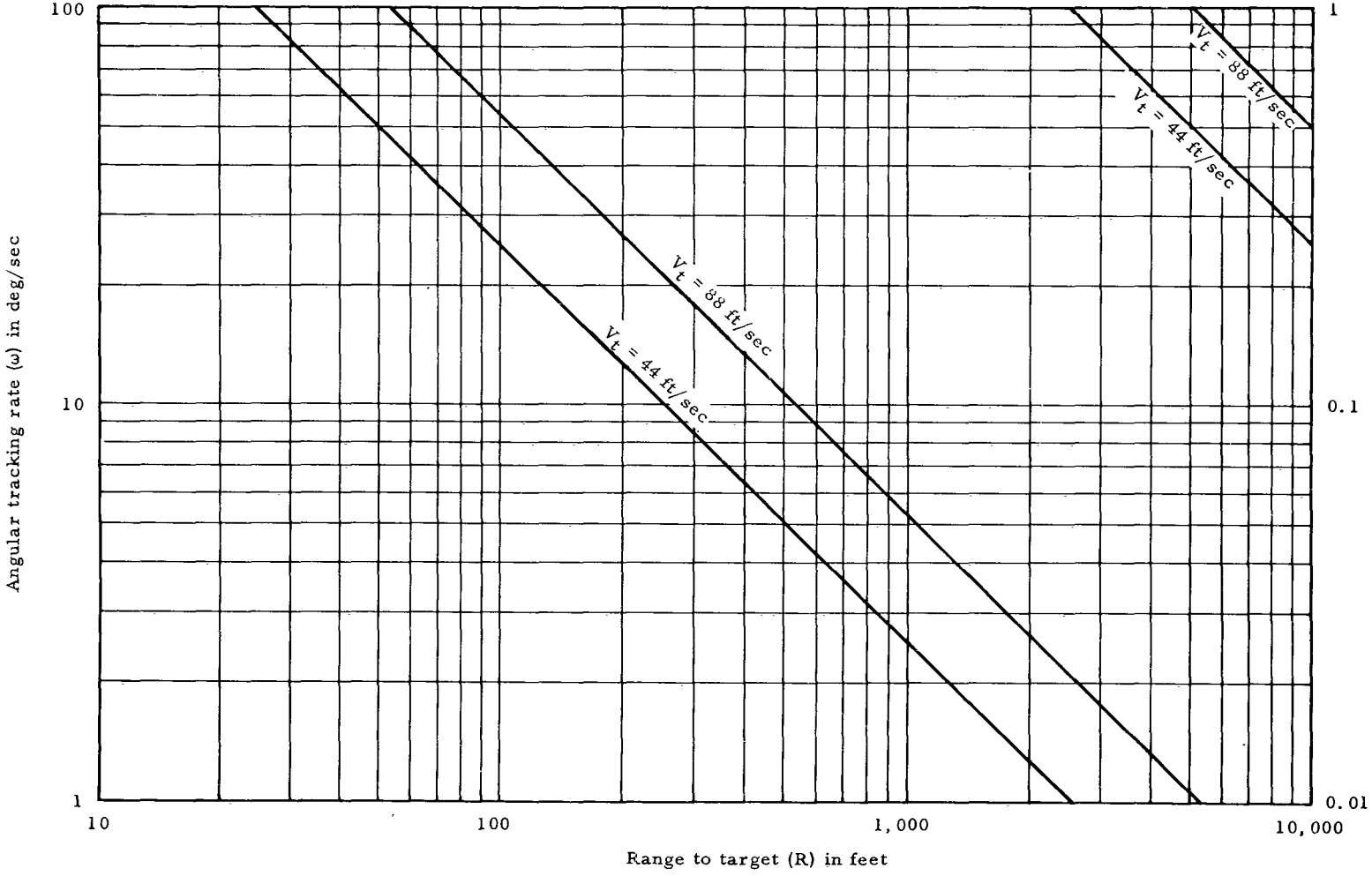

Figure 6. PLOT OF ω VERSUS RANGE.

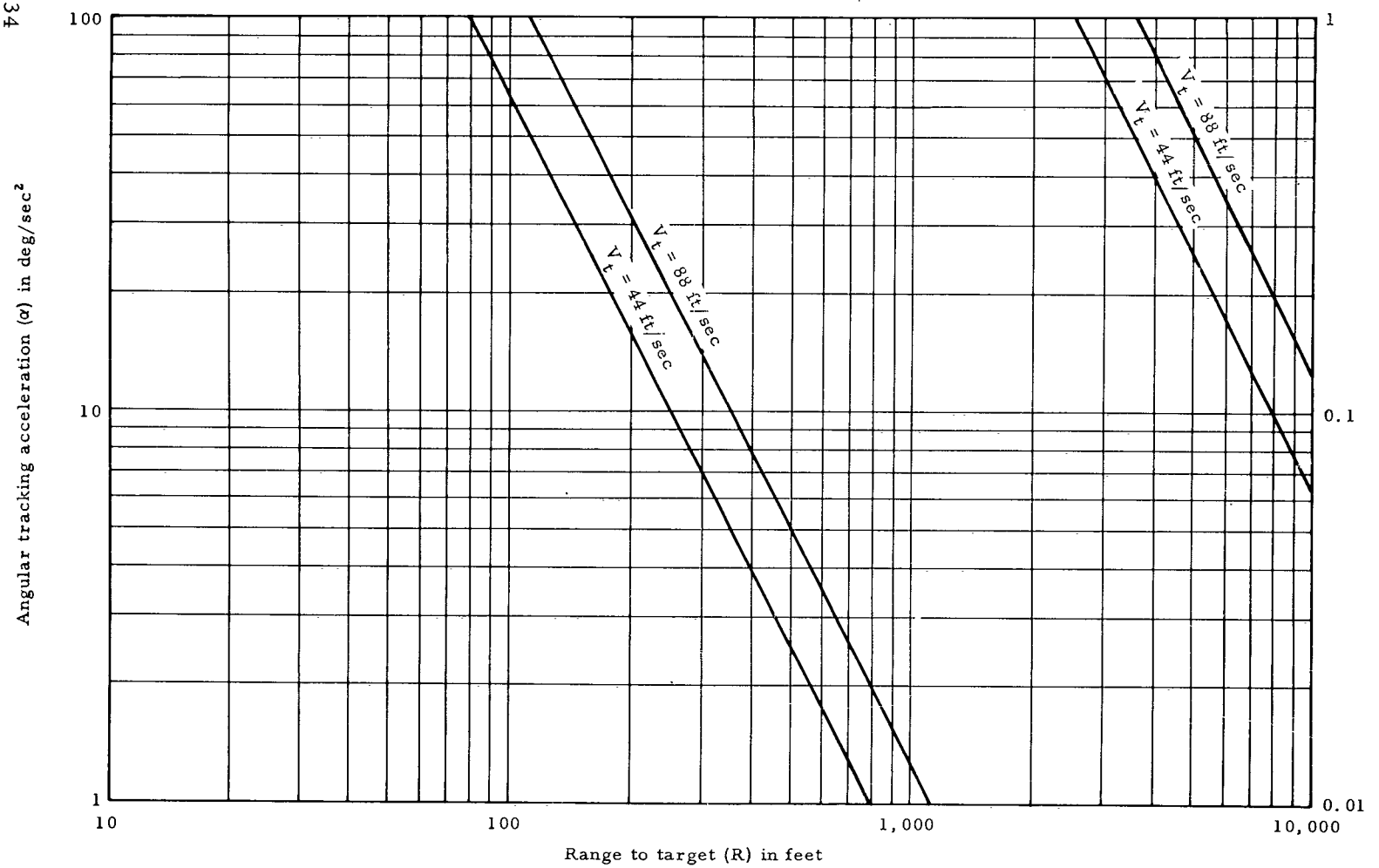

Figure 7. PLOT OF α VERSUS RANGE.

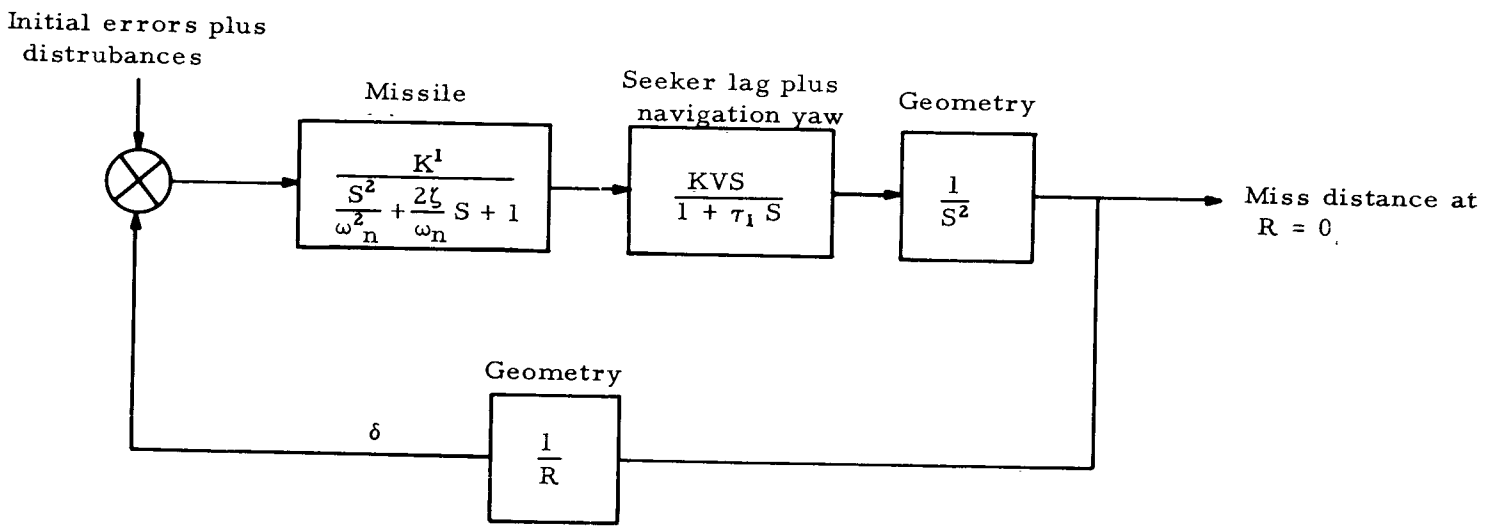

Figure 8. BLOCK DIAGRAM OF SIMPLE HOMING LOOP

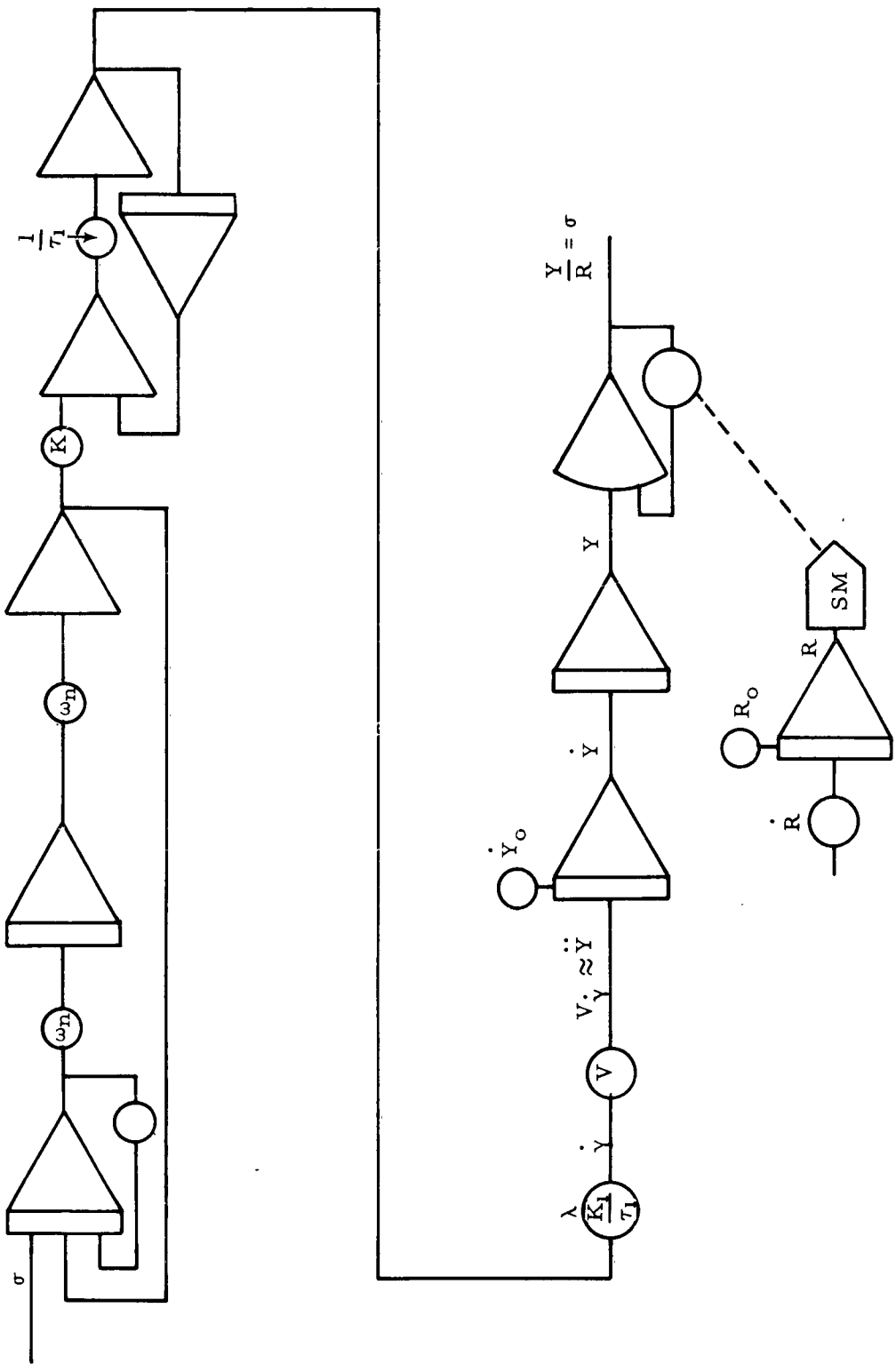

Figure 9. COMPUTER DIAGRAM FOR SIMPLE HOMING LOOP.

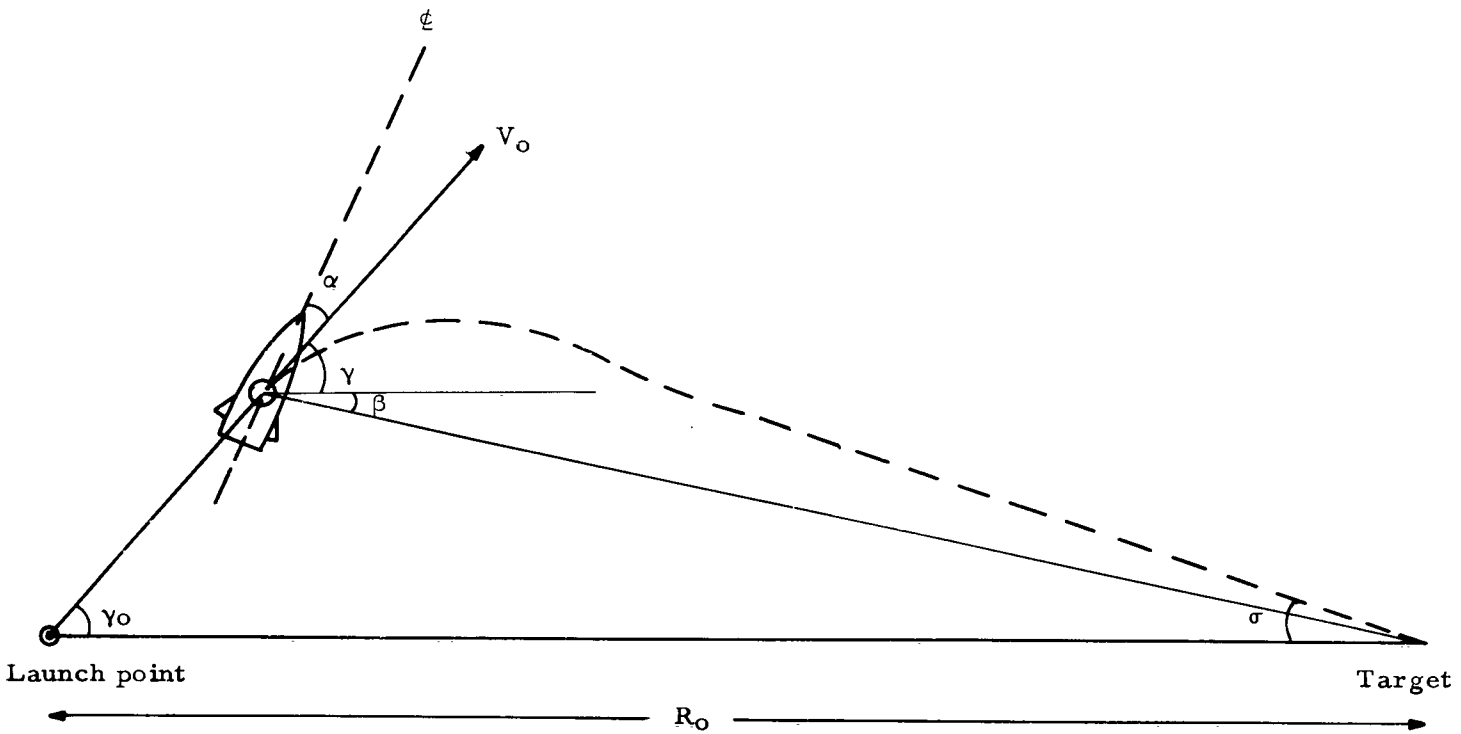

Figure 10. EXAGGERATED LAUNCH GEOMETRY (YAW).

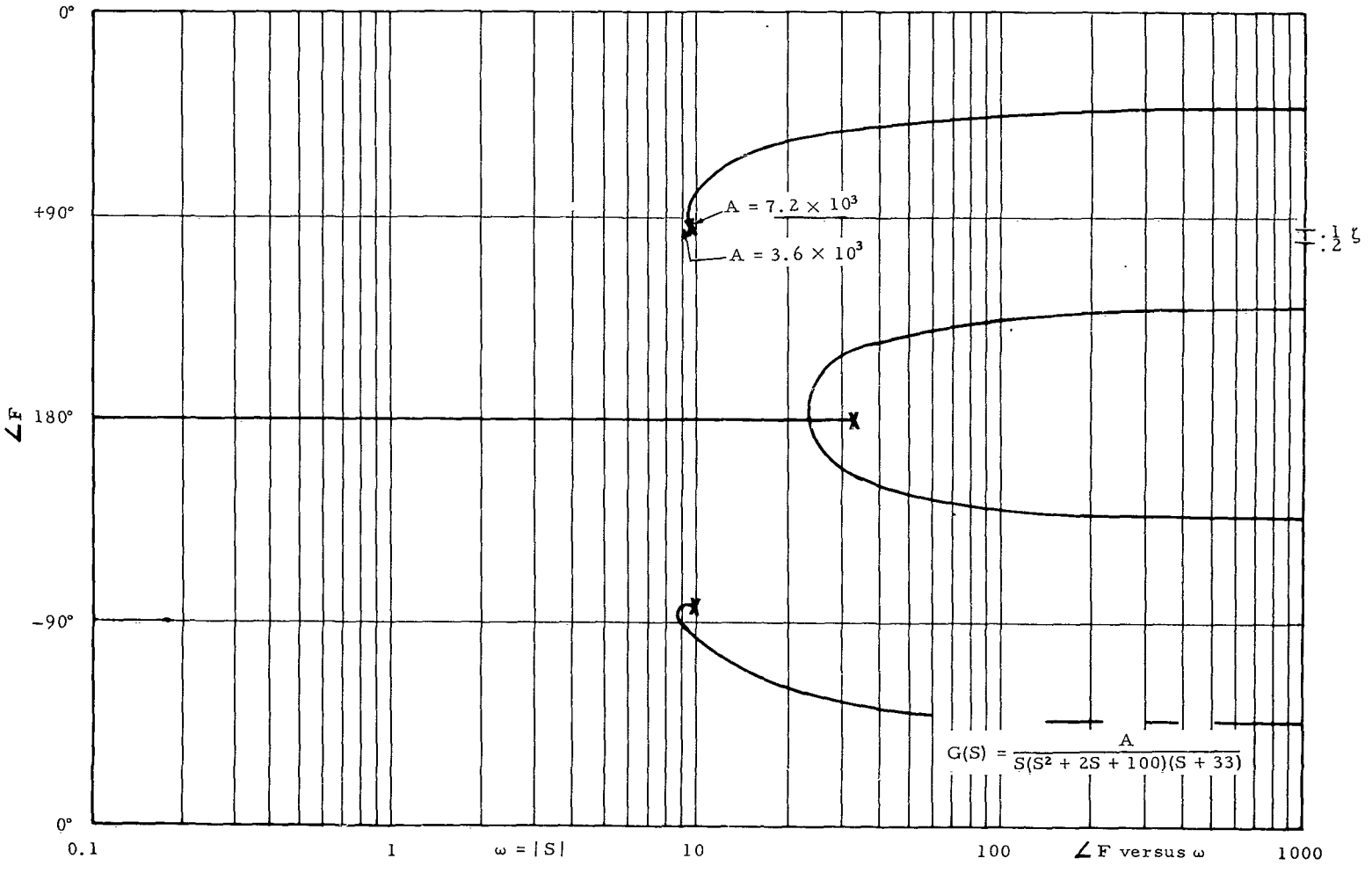

Figure 11. ROOT LOCUS PLOT FOR A TYPICAL MISSILE MODEL.

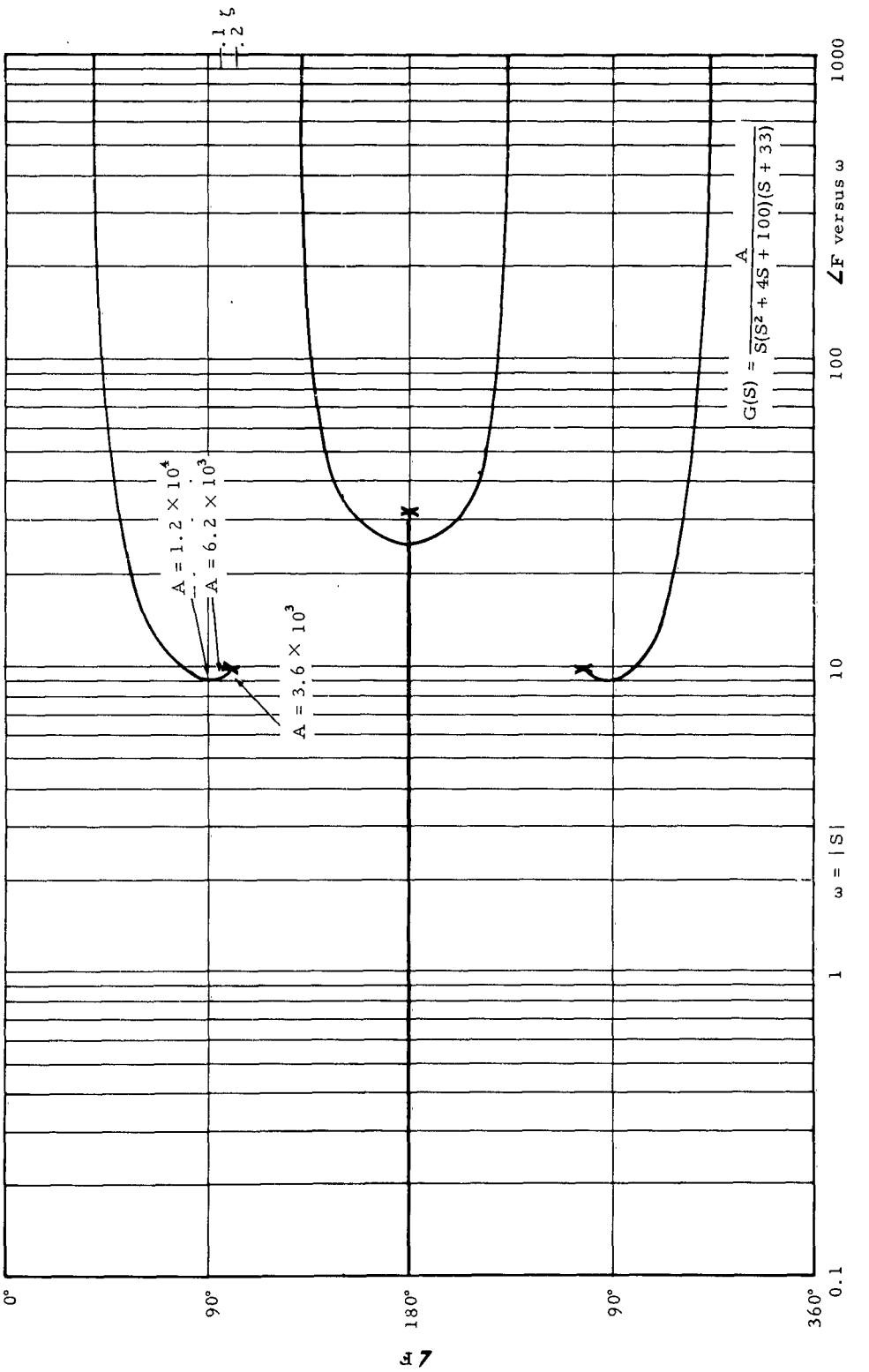

Figure 12. ROOT LOCUS PLOT FOR A TYPICAL MISSILE MODEL.

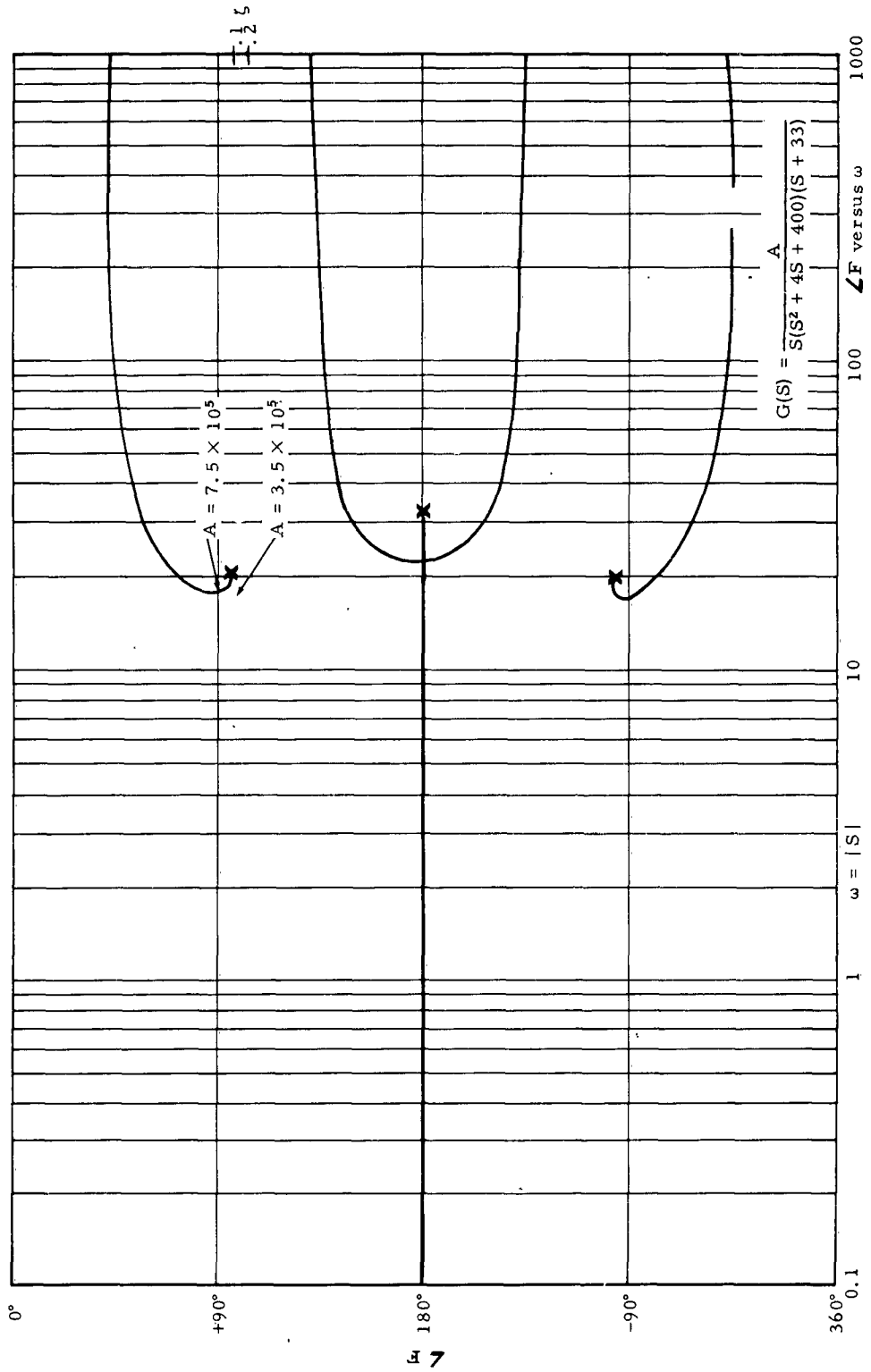

Figure 13. ROOT LOCUS PLOT FOR A TYPICAL MISSILE MODEL.

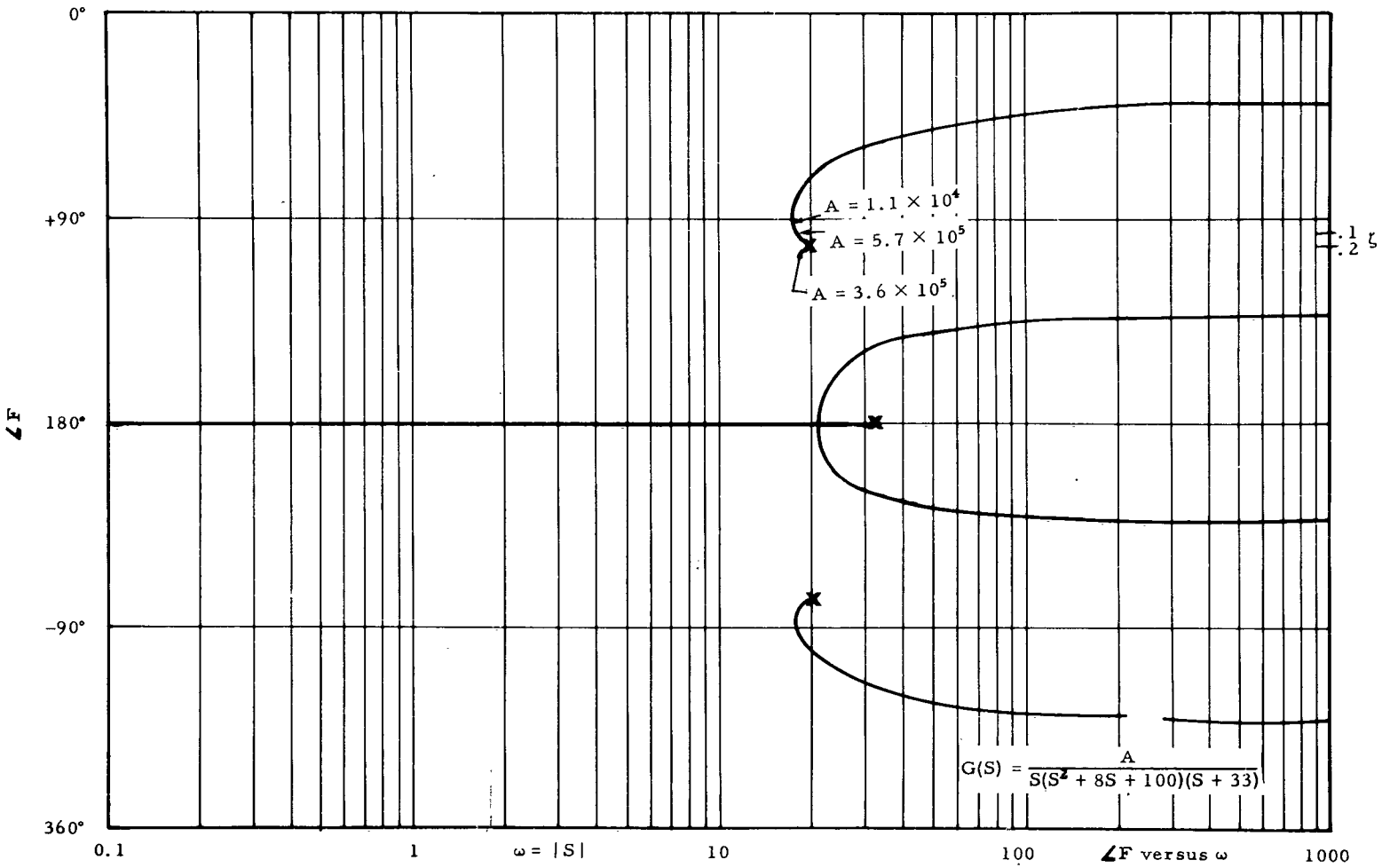

Figure 14. ROOT LOCUS PLOT FOR A TYPICAL MISSILE MODEL.

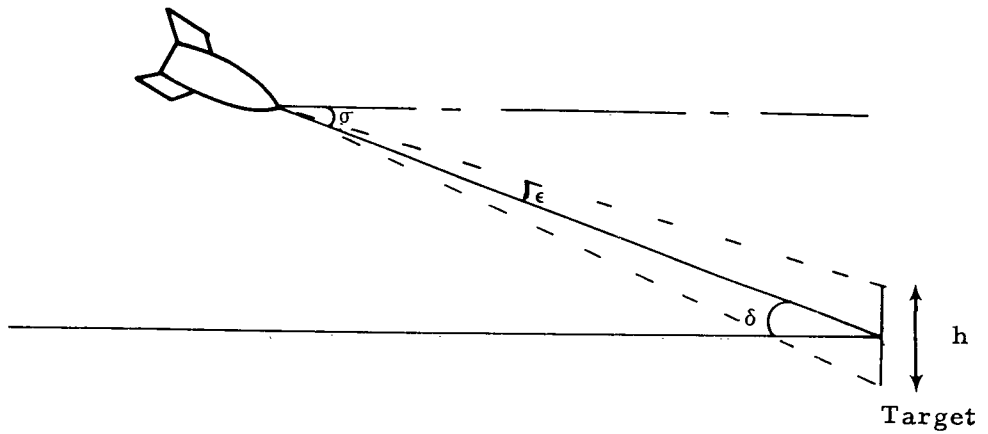

Figure 15. TERMINAL GEOMETRY SHOWING ANGLE ϵ.

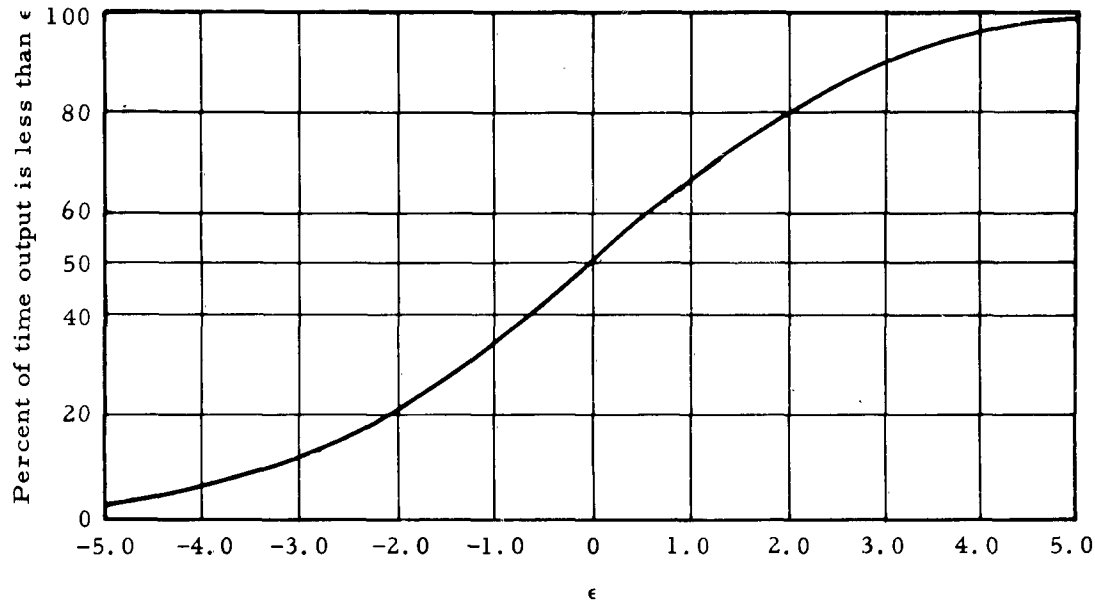

Figure 16. CUMULATIVE PROBABILITY DISTRIBUTION OF ϵ FOR S/N = 7.

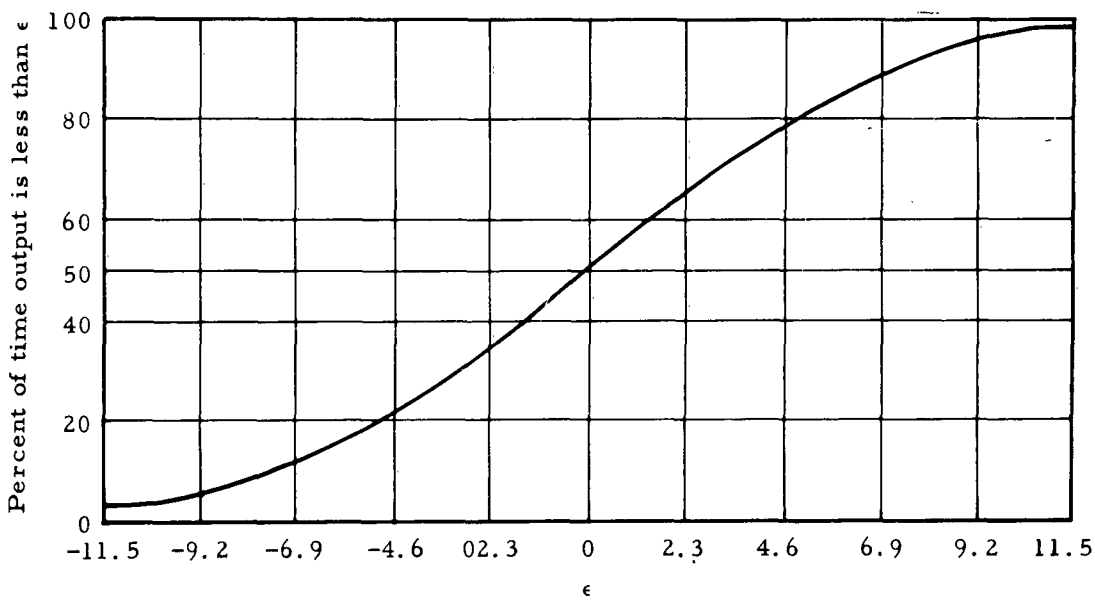

Figure 17. CUMULATIVE PROBABILITY DISTRIBUTION OF ϵ FOR S/N = 3.5

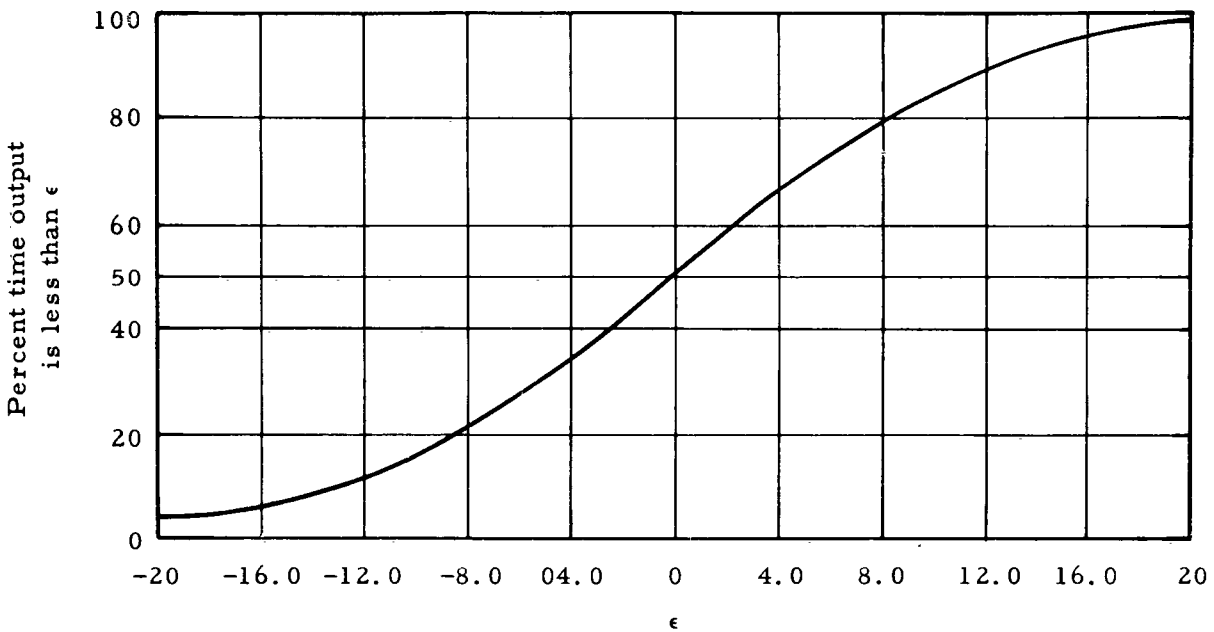

Figure 18. CUMULATIVE PROBABILITY DISTRIBUTION OF ϵ FOR S/N 2.

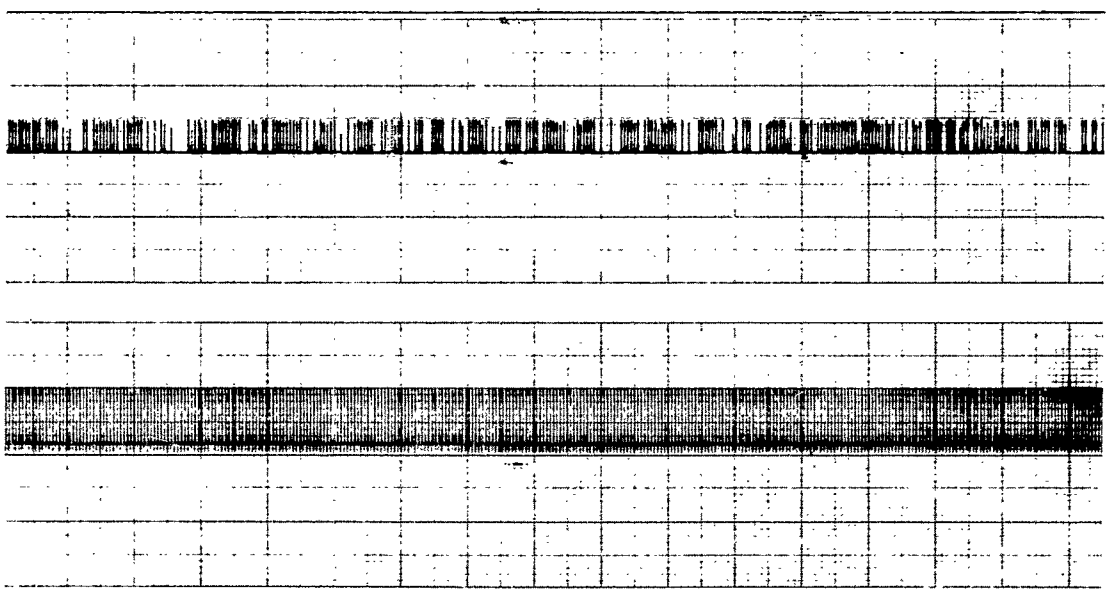

Figure 19. SAMPLE PLOT FOR EXPERIMENTAL P_h DETERMINATION.

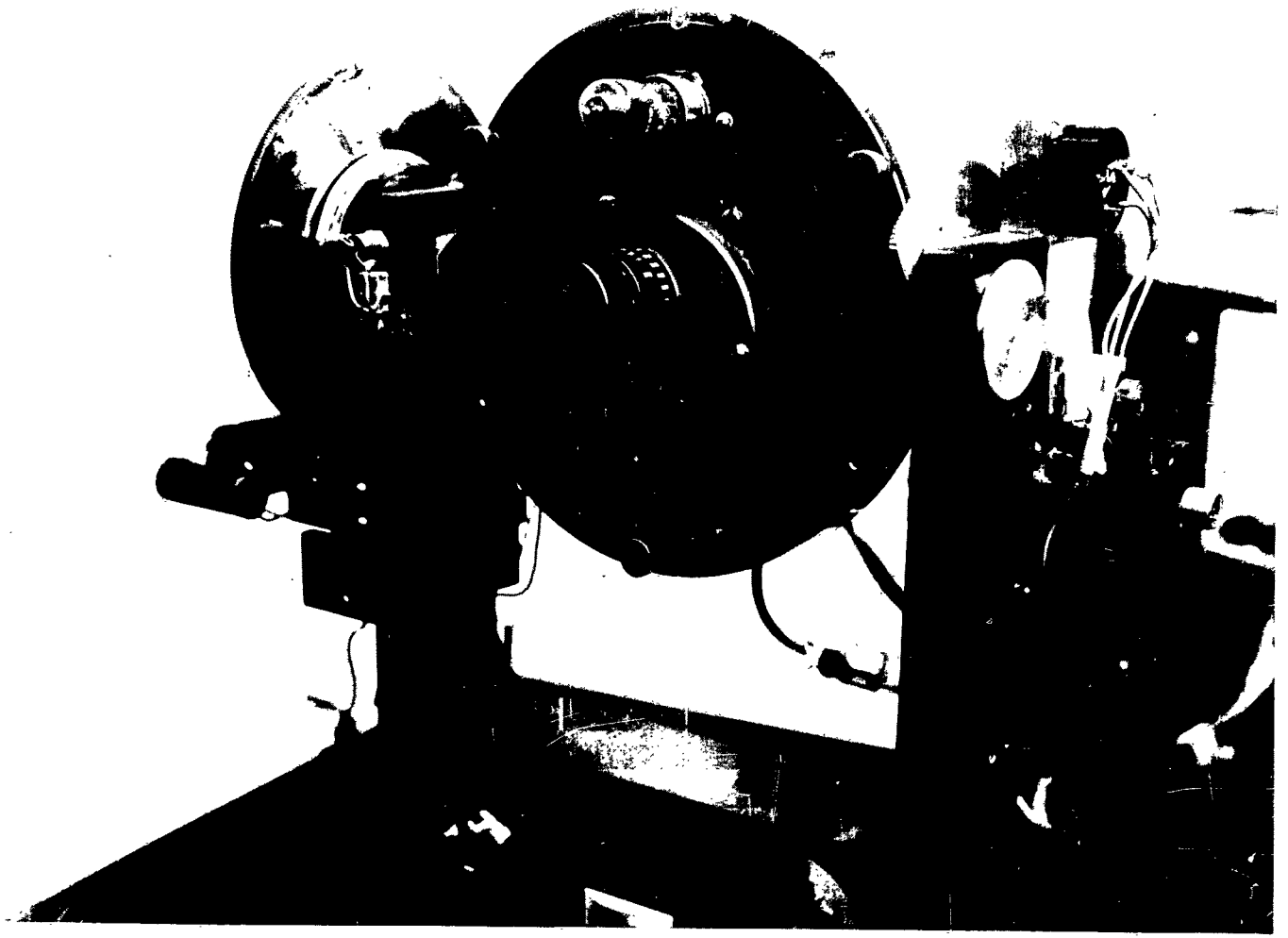

Figure 20. PHOTOGRAPH SHOWING TV SERVO TRACKER.

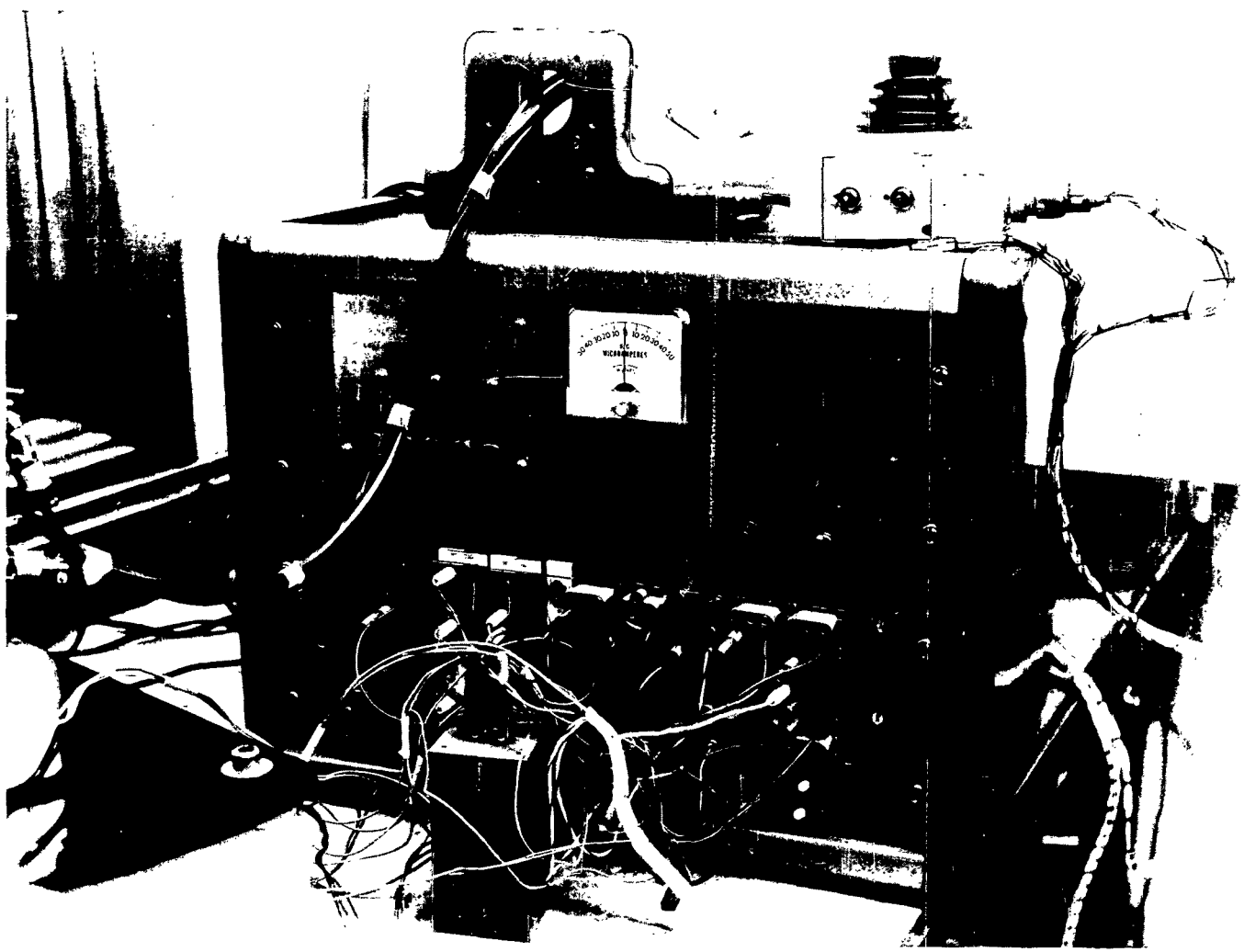

Figure 21. PHOTOGRAPH SHOWING TRACKER ELECTRONICS.

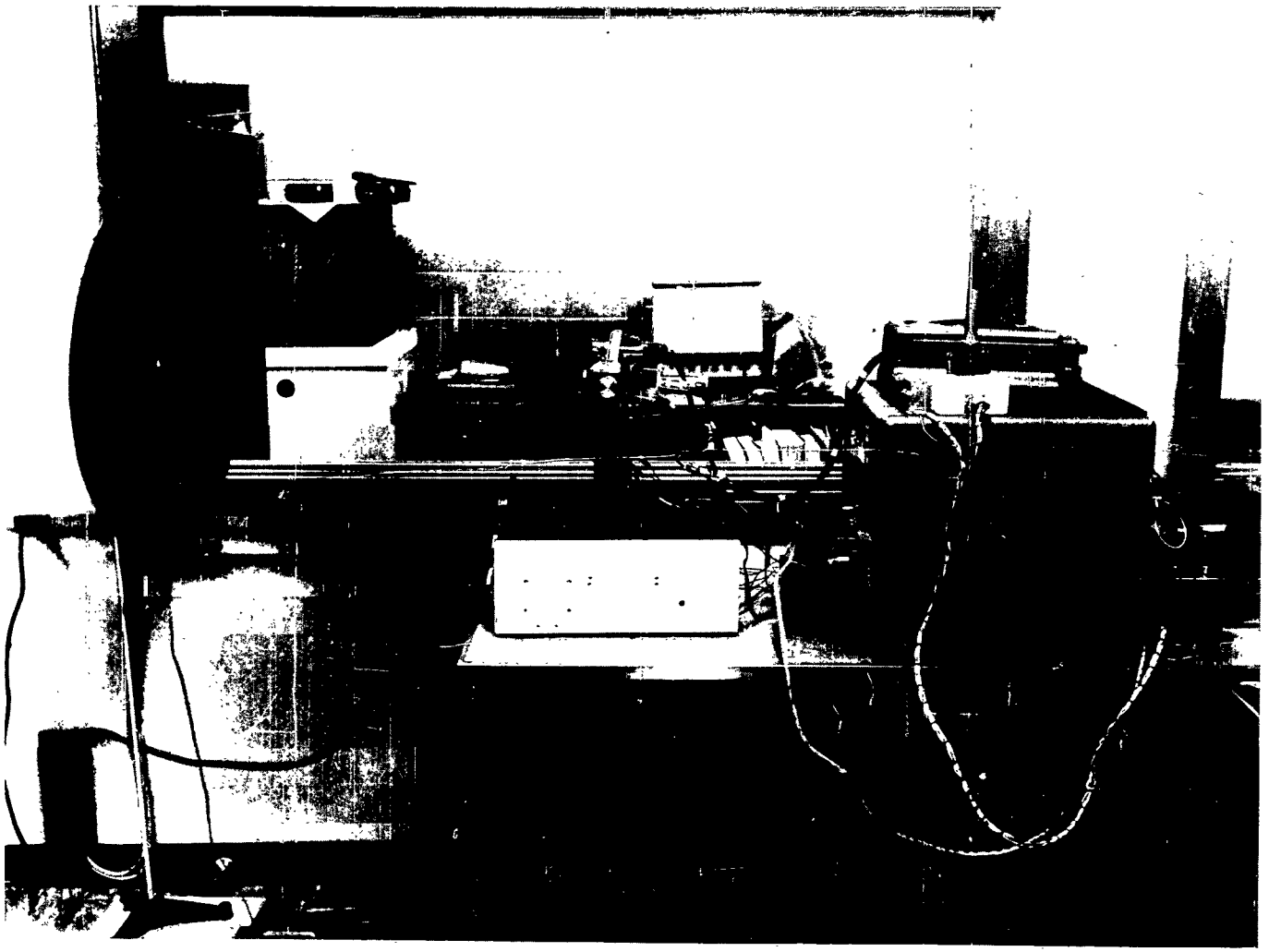

Figure 22. PHOTOGRAPH SHOWING TRACKING EXPERIMENT.

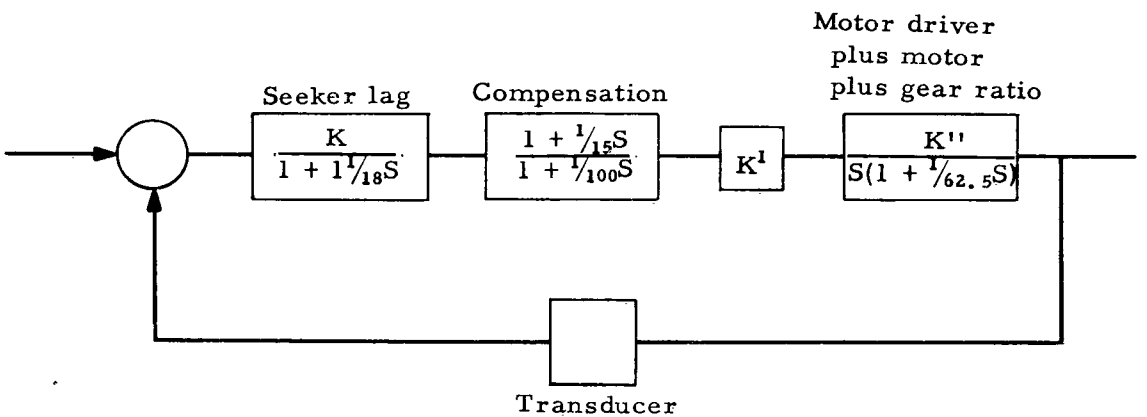

Figure 23. TRACKER BLOCK DIAGRAM.

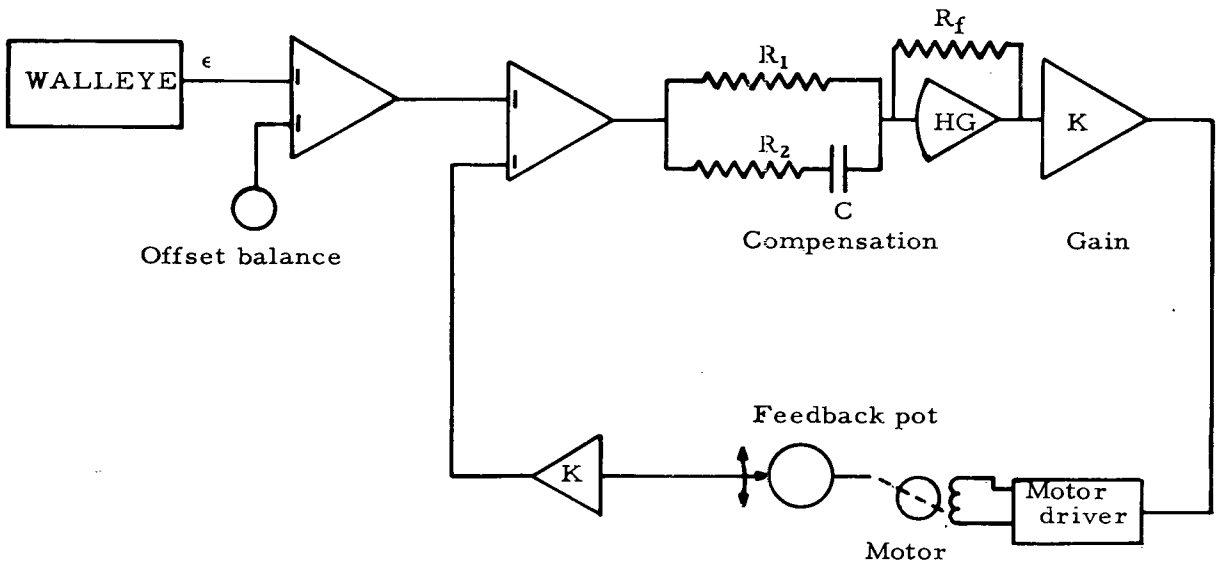

Figure 24. SERVO LOOP, SIMPLIFIED SCHEMATIC

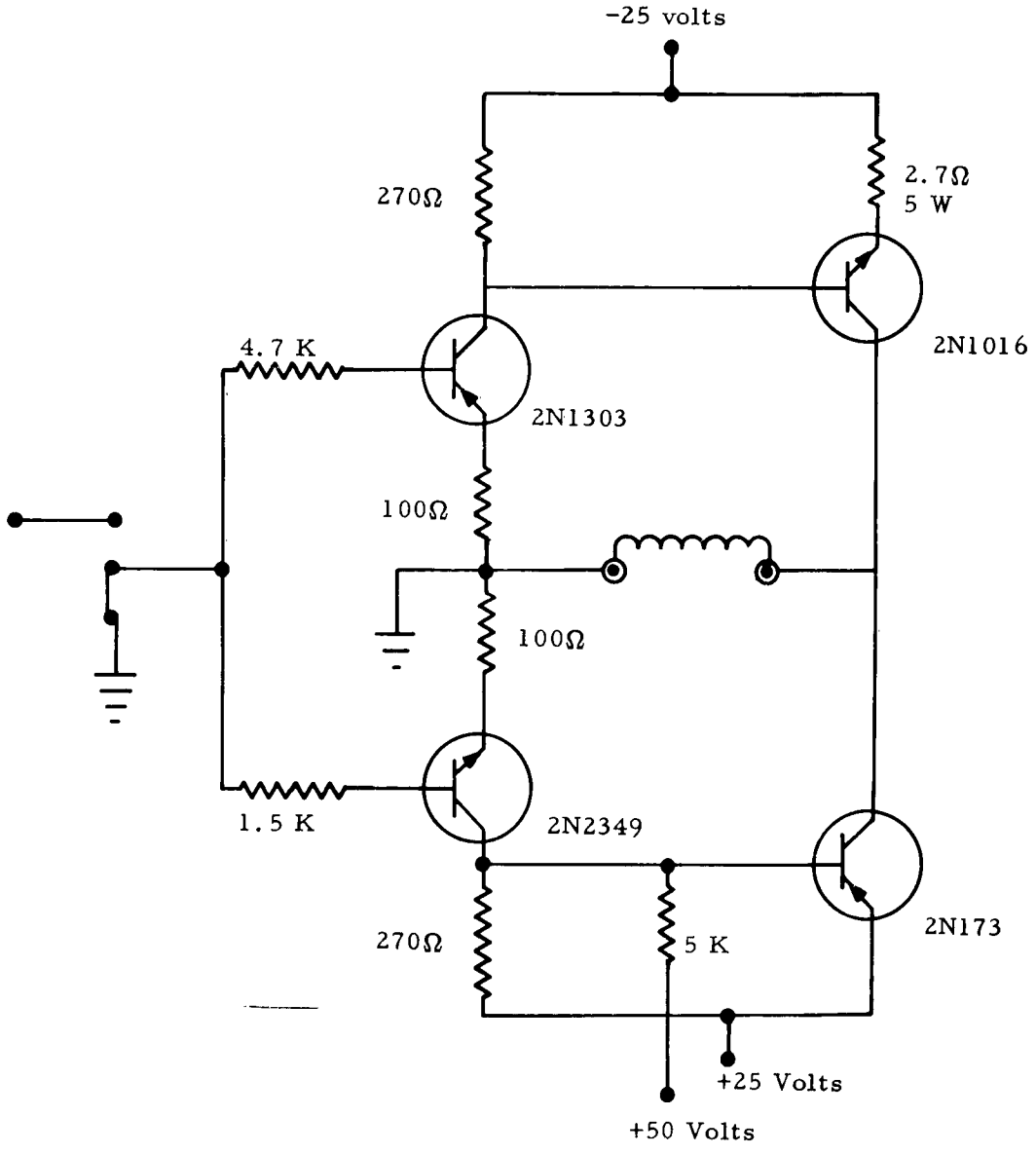

Figure 25. MOTOR DRIVER

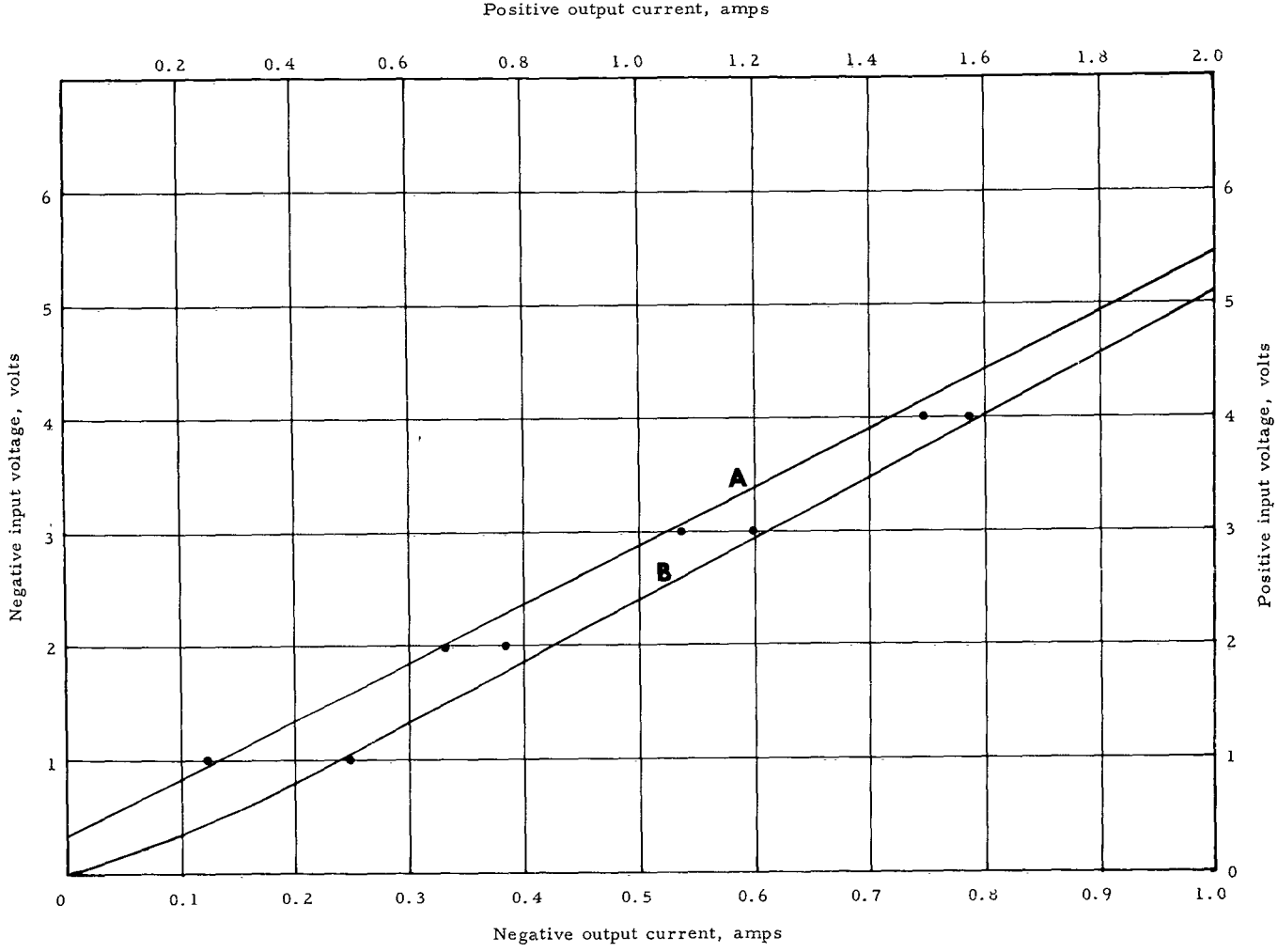

Figure 26. MOTOR DRIVEN AMPLIFIER GAIN FUNCTION.

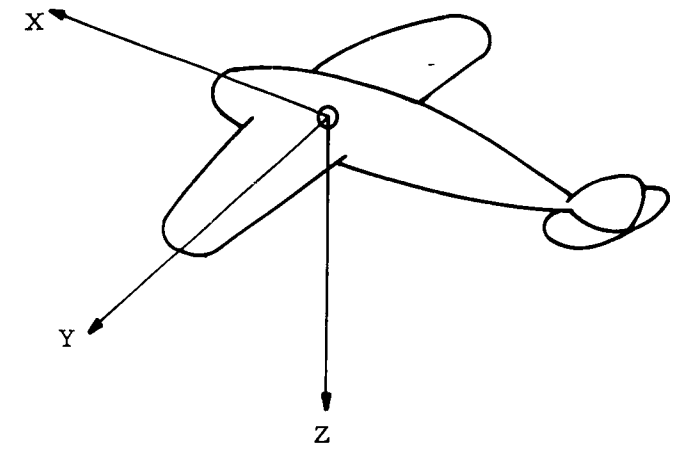

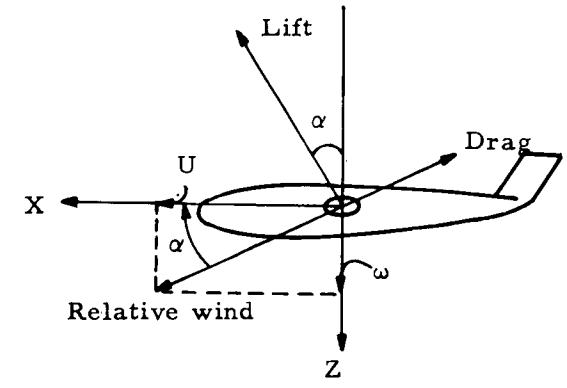

Figure B-1. WINGED VEHICLE CORDINATES AND GEOMETRY.

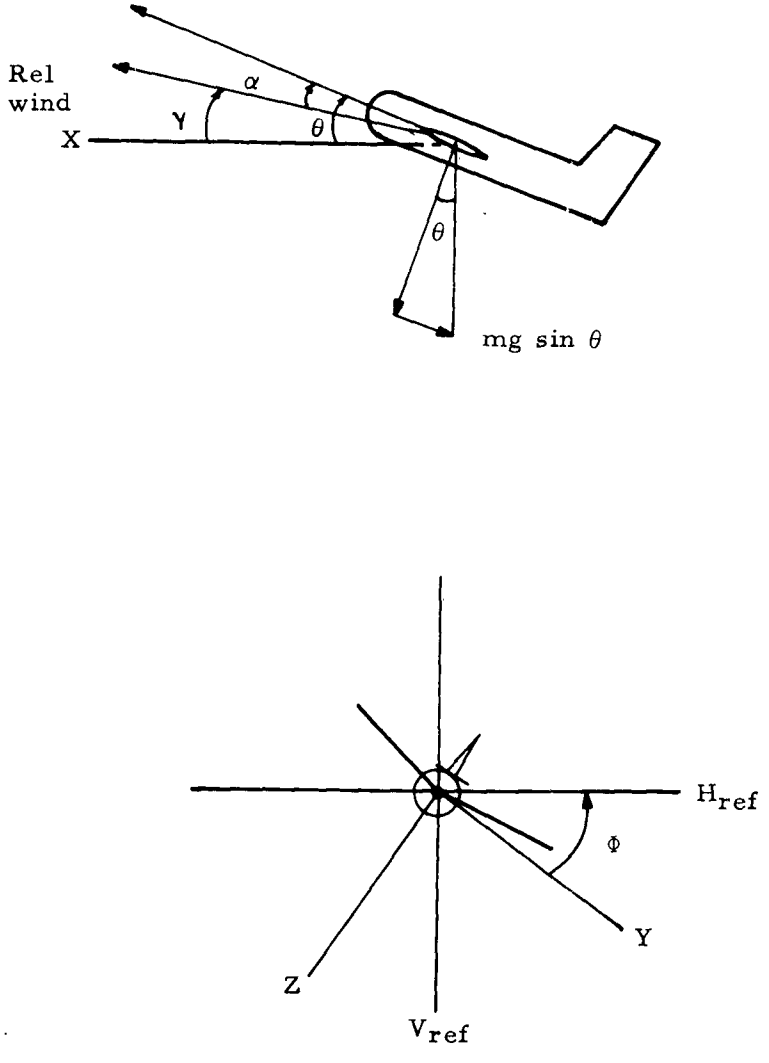

Figure B-2. WINGED VEHICLE PITCH AND ROLL GEOMETRY.

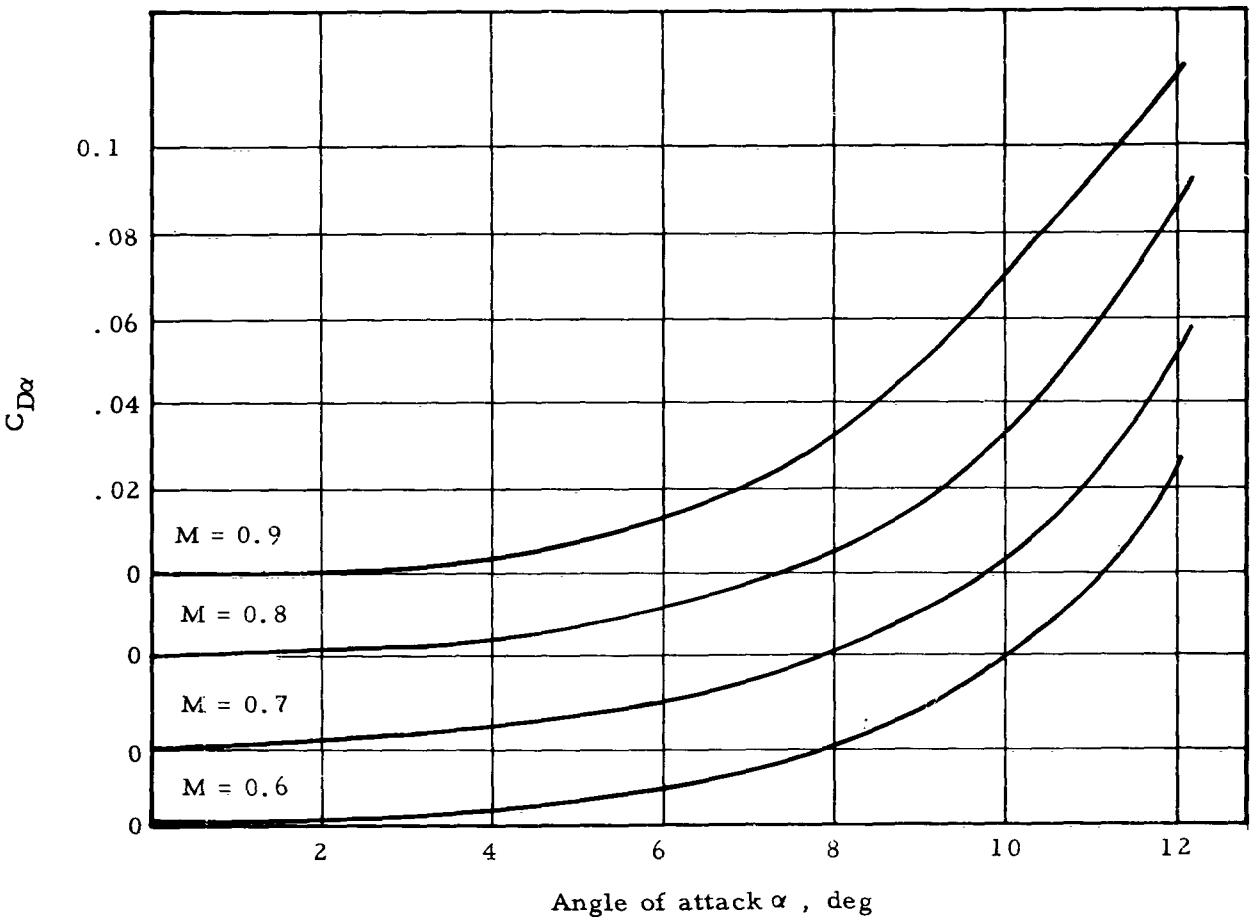

Figure B-3. DRAG VERSUS ANGLE OF ATTACK.

REFERENCES

1. Adler, F. P.: "Missile Guidance by Three-dimensional Proportional Navigation", J. Appl. Phys., vol. 27, no. 5 (May, 1956).

2. Del Toro and Parker, Principles of Control Systems Engineering, McGraw-Hill, 1960.

3. Ryan Aeronautical Company, Report 12454-1, 1 July 1962, "Final Stability and Control Derivatives Report. USAF XQ-2C Target Drone".

APPROVAL:

JACK ZAROVSKY
Chief, Correlation Branch

for DELMAR E. ROWE
Director, Electromagnetics Laboratory

DISTRIBUTION

	Copy
Commander Defense Documentation Center for Scientific and Tech Info. Arlington Hall Station Arlington 12, Virginia Attn: TIPCR	1-10
Chief, Air Defense Division Office, Chief of Research and Development Department of the Army The Pentagon, Room 3E 371 Washington 25, D. C.	11
Director Air University Library Maxwell Air Force Base, Alabama Attn: AUL3T	12
Commander Aeronautical Systems Division Wright-Patterson Air Force Base, Ohio Attn: ASAPRD-Dist.	13-17
Commander Rome Air Development Center (RAALD) Griffiss Air Force Base, New York Attn: Documents Library	18
Commanding Officer (AD-5) U. S. Naval Air Development Center Johnsville, Pennsylvania Attn: NADC Library	19
Commanding Officer U. S. Army Research Office Box CM, Duke Station Durham, North Carolina Attn: CRD-AA-IP	20
Library U. S. Army War College Carlisle Barracks, Pennsylvania	21

DISTRIBUTION (Continued)

	Copy
Commanding Officer U. S. Army Infantry Combat Developments Agency Fort Knox, Kentucky	22
Commanding Officer U. S. Army Infantry Combat Developments Agency Fort Benning, Georgia	23
Commanding General U. S. Army Electronics Command Fort Monmouth, New Jersey Attn: AMSEL-CB	24
Director, Research Analyses Holloman Air Force Base, New Mexico Attn: Technical Library (SRAT)	25
Director, Weapons Systems Evaluation Group Room 1E 875, The Pentagon Washington 25, D. C.	26
Commanding General White Sands Missile Range, New Mexico Attn: Technical Library	27-30
Commanding Officer Rock Island, Illinois Attn: SWERI-RDI-Document Section	31
Office, Assistant Secretary of the Army (R&D) Room 3E 390, The Pentagon Washington 25, D. C.	32
Superintendent U. S. Naval Postgraduate School Monterey, California Attn: Code 0384	33
Scientific and Technical Information Facility P. O. Box 5700 Bethesda, Maryland Attn: NASA Representative (S-AK/DL)	34-38

DISTRIBUTION (Continued)

	Copy
Director National Security Agency Fort George G. Meade, Maryland Attn: C3/TDL (Room 2C087)	39
Commanding Officer Diamond Ordnance Fuze Laboratories Washington 25, D. C. Attn: Technical Reference Branch	40
Director, Guided Missile Department U. S. Army Artillery and Missile School Fort Sill, Oklahoma	41
Commanding Officer U. S. Army Office of Special Weapons Development U. S. Army Combat Developments Command Fort Bliss 16, Texas	42
Commandant U. S. Army Command and General Staff College Fort Leavenworth, Kansas Attn: Archives	43
Director U. S. Naval Research Laboratory Washington 25, D. C. Attn: Code 2027	44
U. S. Army Air Defense Engineering Agency Fort George G. Meade, Maryland Attn: SELAD-6B	45
Commander U. S. Naval Ordnance Laboratory White Oak Silver Spring, Maryland Attn: Librarian	46, 47
Technical Library Naval Weapons Laboratory Dahlgren, Virginia	48

DISTRIBUTION (Concluded)

	Copy
Commanding General U. S. Army Materiel Command Washington 25, D. C. Attn: AMCCG AMCRD	49, 50
Central Intelligence Agency Washington 25, D. C. Attn: OCR - Standard Distribution	51-54
Headquarters U. S. Army Test and Evaluation Command Aberdeen Proving Ground, Maryland Attn: AMSTE	55
Director Missile Division U. S. Army Artillery Board Fort Sill, Oklahoma	56
Commanding General U. S. Army Missile Command Redstone Arsenal, Alabama Attn: USACDC LnO	57
AMSMI-R, Attn: Mr. McDaniel	58
-RF, Attn: Mr. Salonimer	59-63
-RR	64
-RG	65
-RE	66
-RES	67-69
-REO	70-72
-RB	73-77
-RAP	79

AD_____ Accession No._____ Army Missile Command, Directorate of Research and Development, Electromagnetics Laboratory, Redstone Arsenal, Alabama SOME OPTICAL CONTRAST SEEKER SYSTEM CONSIDERATIONS - G. Willems Army Msl Cmd RE-TR-62-10, 31 Dec 62, 61 pp - illus. Unclassified Report Some elementary problems peculiar to a ground-to-ground homing missile system are discussed. The work is specifically oriented toward the application of a television guidance sensor of the contrast contour type to an antitank weapon. The design of a simple laboratory TV servo-tracker is presented. Parameters pertinent to XQ-2 drone are given.	UNCLASSIFIED 1. Antitank weapons--Guidance 2. Optical seekers 3. Servo tracker--Design 4. Targets--Acquisition 5. Targets--Identification 6. Television guidance--Application 7. XQ-2--Motion I. Willems, G. DISTRIBUTION: Copies obtainable from DDC, Arlington Hall Station, Arlington 12, Virginia.	AD_____ Accession No._____ Army Missile Command, Directorate of Research and Development, Electromagnetics Laboratory, Redstone Arsenal, Alabama SOME OPTICAL CONTRAST SEEKER SYSTEM CONSIDERATIONS - G. Willems Army Msl Cmd RE-TR-62-10, 31 Dec 62, 61 pp - illus. Unclassified Report Some elementary problems peculiar to a ground-to-ground homing missile system are discussed. The work is specifically oriented toward the application of a television guidance sensor of the contrast contour type to an antitank weapon. The design of a simple laboratory TV servo-tracker is presented. Parameters pertinent to XQ-2 drone are given.	UNCLASSIFIED 1. Antitank weapons--Guidance 2. Optical seekers 3. Servo tracker--Design 4. Targets--Acquisition 5. Targets--Identification 6. Television guidance--Application 7. XQ-2--Motion I. Willems, G. DISTRIBUTION: Copies obtainable from DDC, Arlington Hall Station, Arlington 12, Virginia.
AD_____ Accession No._____ Army Missile Command, Directorate of Research and Development, Electromagnetics Laboratory, Redstone Arsenal, Alabama SOME OPTICAL CONTRAST SEEKER SYSTEM CONSIDERATIONS - G. Willems Army Msl Cmd RE-TR-62-10, 31 Dec 62, 61 pp - illus. Unclassified Report Some elementary problems peculiar to a ground-to-ground homing missile system are discussed. The work is specifically oriented toward the application of a television guidance sensor of the contrast contour type to an antitank weapon. The design of a simple laboratory TV servo-tracker is presented. Parameters pertinent to XQ-2 drone are given.	UNCLASSIFIED 1. Antitank weapons--Guidance 2. Optical seekers 3. Servo tracker--Design 4. Targets--Acquisition 5. Targets--Identification 6. Television guidance--Applications 7. XQ-2--Motion I. Willems, G. DISTRIBUTION: Copies obtainable from DDC, Arlington Hall Station, Arlington 12, Virginia.	AD_____ Accession No._____ Army Missile Command, Directorate of Research and Development, Electromagnetics Laboratory, Redstone Arsenal, Alabama SOME OPTICAL CONTRAST SEEKER SYSTEM CONSIDERATIONS - G. Willems Army Msl Cmd RE-TR-62-10, 31 Dec 62, 61 pp - illus. Unclassified Report Some elementary problems peculiar to a ground-to-ground homing missile system are discussed. The work is specifically oriented toward the application of a television guidance sensor of the contrast contour type to an antitank weapon. The design of a simple laboratory TV servo-tracker is presented. Parameters pertinent to XQ-2 drone are given.	UNCLASSIFIED 1. Antitank weapons--Guidance 2. Optical seekers 3. Servo tracker--Design 4. Targets--Acquisition 5. Targets--Identification 6. Television guidance--Application 7. XQ-2--Motion I. Willems, G. DISTRIBUTION: Copies obtainable from DDC, Arlington Hall Station, Arlington 12, Virginia.